공학박사 학위논문

Catalytic Hydrogenation of Alginic Acid into Sugar Alcohols over Ruthenium-based Carbon Catalysts

루테늄 기반 탄소 촉매 상에서 당알코올 생성을 위한 알긴산 수소화 반응

2019년 2월

서울대학교 대학원

화학생물공학부

반 충 현

Abstract

Catalytic Hydrogenation of Alginic Acid into Sugar Alcohols over Ruthenium-based Carbon Catalysts

Chunghyeon Ban

School of Chemical and Biological Engineering

The Graduate School

Seoul National University

Demand for the production of sustainable fuels and chemicals has been growing to alleviate critical environmental issues such as the limited fossil fuel reservoir and fossil fuel-related pollution and to reduce a heavy dependence on petroleum-based chemicals. Biomass is considered to be the most promising renewable resource since organic compounds with basic elements of C, H, O can be directly produced only from biomass. Biomass feedstock is classified into three generations, namely edible food crops (the 1st), lignocellulose (the 2nd), and algae (the 3rd). The first two have been extensively investigated to produce value-added chemicals from them. However, it is only in recent years that the third generation biomass drew attention to produce renewable chemicals for its advantageous features over its terrestrial predecessors such as rapid growth, inedibility, and lignin-free structure. Alginic acid, a major constituent of brown algae, is composed of two epimeric uronic acids,

mannuronic acid and guluronic acid, linked by β-1,4-glycosidic bond.

Sorbitol and mannitol are value-added sugar alcohols that are used not only as a food additive but also as a potential platform chemical to produce hydrogen for fuel cells, vitamin C, glycols, and monomers of polymers. Industrial production of sorbitol is currently realized by hydrogenation of glucose which could be derived from terrestrial biomass such as starch or cellulose. To the best of my knowledge, however, catalytic hydrogenation of macroalgae-derived alginic acid into sugar alcohols has never been investigated. In this work, alginic acid was catalytically converted into sugar alcohols, mainly sorbitol and mannitol, over ruthenium-based carbon catalysts.

Firstly, various noble metals supported on carbon were used for the hydrogenation of alginic acid. Sorbitol and mannitol could be selectively produce over Ru-based carbon catalysts while byproducts (dideoxy-aldonic acids and their lactones) were produced over Pd, Pt, Rh, and Ir supported on carbon. The highest yield of C6 sugar alcohols was 61% (sorbitol: 29%, mannitol: 28%, and galactitol: 4%) at 150 °C for 12 h under 50 bar of H_2 over the commercial ruthenium supported on carbon catalyst. Isomerization between produced sugar alcohols was evidenced by ^{13}C NMR analysis of the reactant, alginic acid, and GC-MS analysis of the products. In addition, based on LC-MS, a plausible reaction pathway for the formation of sugar alcohols from alginic acid was proposed that consecutive hydrogenation of dimeric intermediates with two reducible functional groups (carboxyl- and aldehyde-end) led to the formation of partially hydrogenated intermediates before cleaved into target C6 sugar alcohols. The commercial Ru catalyst exhibited a poor hydrothermal stability, resulting in leaching and

aggregation of Ru.

Secondly, various transition metals were added to Ru supported on nitric acid-treated activated carbon. Among them, Cu-promoted Ru catalyst suppressed the formation of byproducts, short chain sugar alcohols and galactitol, the most. Addition of Cu to Ru caused blocking of active Ru surface and electron transfer between Ru and Cu as evidenced by CO-chemisorption and XPS, respectively. The presence of RuCu bimetallic clusters and the intimate interaction between Ru and Cu expedited hydrogen spillover from Ru to Cu, which enabled such RuCu bimetallic catalyst to maintain its hydrogenation activity despite the decrease in active Ru surface exposed. The highest yield of target C6 sugar alcohols was obtained as 47.4% (sorbitol: 26.9% and mannitol: 20.5%) at 180 °C for 2 h under 50 bar of H_2 over Ru(5)Cu(1)/AC-N-13, where numbers in parenthesis refer to loading amount (wt%) of each metal. RuCu bimetallic catalyst was deactivated over repeated reactions owing to leaching of Cu.

Lastly, to improve hydrothermal stability of the ruthenium-based catalyst, nitrogen-doped mesoporous carbon was synthesized and employed as a support. Nitrogen content was controlled by changing weight ratio of urea/glucose and carbonization temperature. The introduction of nitrogen induced the interaction of Ru with the support, especially with pyridinic-N, which led to the formation of RuO_x species. In addition, the intimate interaction between ruthenium and N-doped carbon facilitated hydrogen spillover from Ru to the support. The oxidized Ru was found to suppress side reactions such as epimerization and C-C cleavage. The highest yield of target C6 sugar alcohols was 50.3% (sorbitol: 24.3% and mannitol: 26.0%) at 180 °C for 1 h under 50 bar of H_2 over Ru(5)/NMC(0.1)(600), where 0.1 and 600

refer to urea/glucose ratio and carbonization temperature (°C), respectively. The catalyst exhibited excellent hydrothermal stability under pressurized H_2. A strong interaction was proposed to be the origin of the inhibition of leaching and aggregation of Ru.

This first attempt to utilize alginic acid as a promising surrogate for cellulose to produce sugar alcohols would alleviate the heavy dependence on lignocellulosic biomass and pave the way for diversifying biomass resources.

Keywords**:** Alginic acid, hydrogenation, sugar alcohol, ruthenium catalyst, bimetallic catalyst, nitrogen-doped mesoporous carbon

Student Number: 2015-30213

Contents

List of Schemes

List of Figures

List of Tables

Chapter 1. Introduction

1.1. Valorization of biomass resources

Demand for the development of renewable chemicals has been growing to cope with the depletion of the fossil fuel reservoir and to reduce a heavy dependence on petroleum-based chemicals, thus alleviating environmental issues. Among various renewable resources, biomass is considered as the only renewable source of organic carbon that can be directly converted to value-added chemicals [1-2]. To date, a wide variety of biomass such as agricultural crops, wood, and algae have been investigated. Especially, lignocellulosic biomass, composed mainly of cellulose, hemicellulose, and lignin, has been frequently utilized for the production of green fuels and chemicals for the decades [3].

1.2. Catalytic conversion of cellulose into sugar alcohols

Among various lignocellulosic biomass, cellulose has extensively been studied to produce useful building block chemicals. Cellulose, comprising 40-50% of woody biomass by weight, is composed of glucose via β-1,4-glycosidic bond. As shown in Scheme 1-1, for instance, various researches have unveiled strategies to produce valuable platform chemicals from cellulose such as 5-hydroxymethyl furfural [4], lactic acid [5], and levulinic acid [6] which were classified as versatile building block chemicals by U.S. department of energy [7]. The selective production of such value-added chemicals can be realized by the use of catalysts. A myriad of heterogeneous

catalysts such as zeolites, metal oxides, polymer-based resins, and carbon-based materials were employed for the catalytic conversion of cellulose over the last century [8]. In particular, carbon-based catalysts were reported to be well-qualified for the hydrolytic conversion of biomass due to its high hydrothermal stability [9-11]. For instance, cellulose could be hydrolyzed to produce glucose selectively over various carbon-based heterogeneous catalysts such as sulfonated activated carbons [12] and metals supported on mesoporous carbon [13]. Furthermore, glucose could be further hydrogenated to produce sugar alcohols such as sorbitol and mannitol. These C6 sugar alcohols are regarded as a potential building block chemical for the production of vitamin C, ethylene glycol, propylene glycol, and isosorbide or isomannide which are to be utilized for the production of commodity chemicals as displayed in Scheme 1-2 [7]. The commercial production of sorbitol and mannitol occurs by hydrogenation of sugars, such as glucose and fructose, over Raney nickel catalysts, where the sugars are being derived from components of terrestrial biomass such as starch and sucrose [14-15]. However, the use of nickel suffers from the leaching which causes problems in catalyst deactivation and purification of end-products [14]. Therefore, other catalysts such as Ru, Pd, and Pt are being investigated for hydrogenation of sugars and cellulose [16]. For instance, sorbitol was successfully produced from cellulose via hydrogenation over Ru supported on MCM-48, activated carbon, and acid-functionalized silica [17-19].

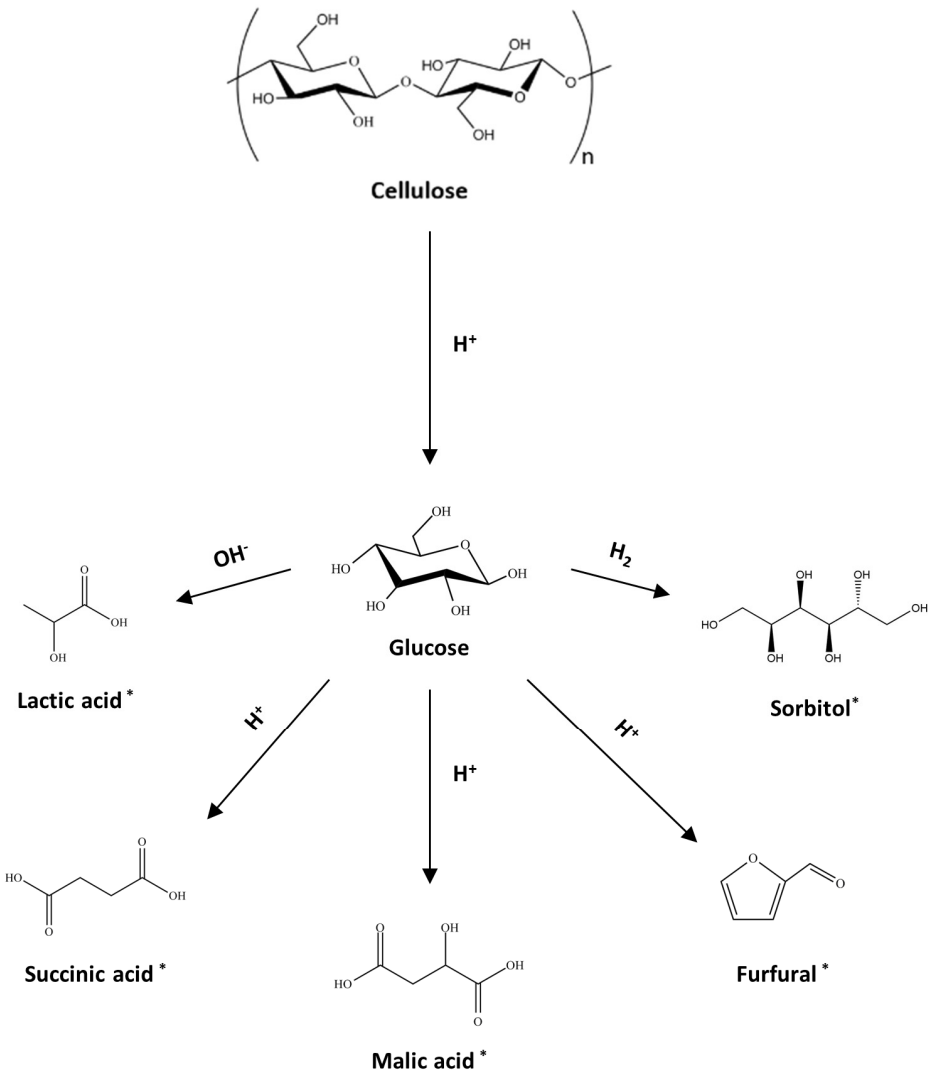

* Top 30 value-added platform chemicals selected by U.S. Department of Energy (2004) [7]

Scheme 1-1. Catalytic conversion of cellulose into building block chemicals.

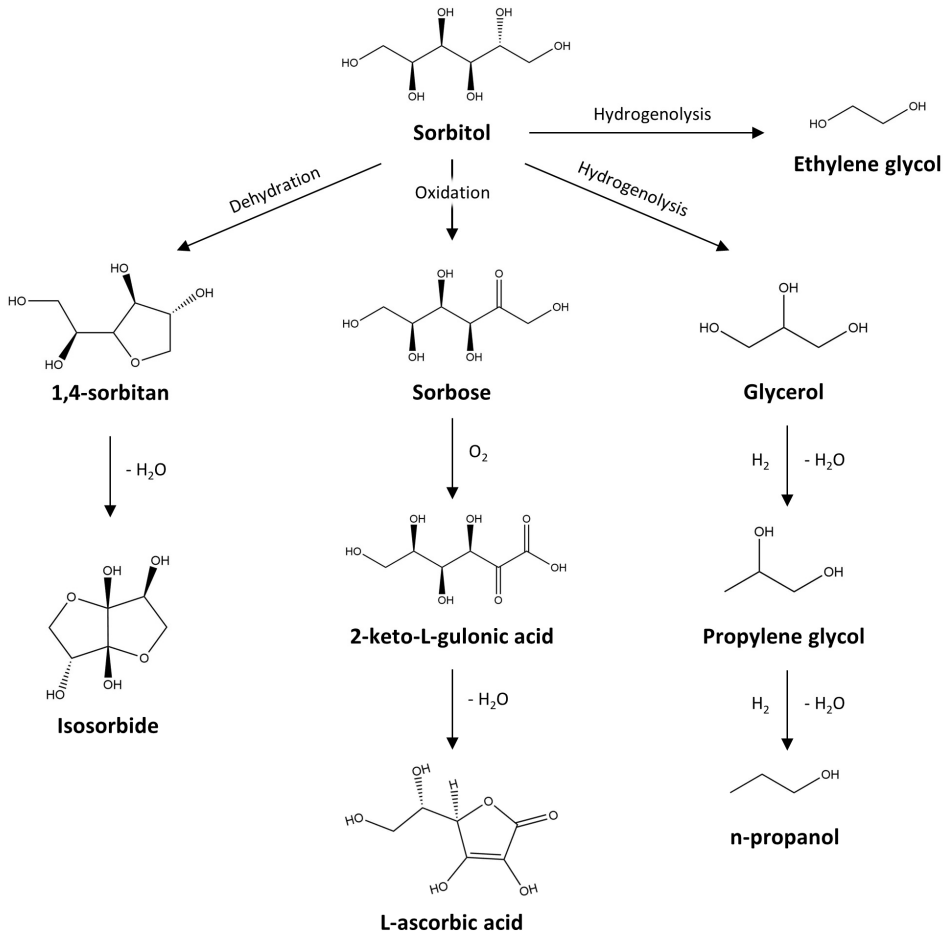

Scheme 1-2. Conversion of sorbitol as a platform chemical into valuable chemicals.

1.3. Catalytic conversion of alginic acid

Recently, algae, known as the third generation biomass, has attracted world-wide attention to replace its terrestrial cousin, lignocellulosic biomass, for the production of renewable fuels and chemicals [20]. The utilization of algal biomass could benefit from advantageous features such as inedibility, rapid growth, and lignin-free structure, compared to its former generations such as agricultural crops and wood [21-22]. As shown in Scheme 1-3, alginic acid, a major constituent of brown-algae, consists of two hexuronic acids, mannuronic acid (M) and guluronic acid (G), via β-1, 4-glycosidic bond which is analogous to the structure of cellulose composed of glucose by the ether bond [23-24]. The ratio of M/G varies with the season, location, and species [25-26].

It is only in recent years that alginic acid has found its new application in the field of biorefinery industries to produce biofuels and chemicals [27-33], further to its traditional applications in the food, medical, and pharmaceutical industries [26]. Recent studies reported that valuable platform chemicals could be produced from alginic acid via catalytic hydrothermal treatment as shown in Scheme 1-4 [27-33]. For example, uronic acids, furfural, and lactic acid were produced from alginic acid over sulfonated carbons, heteropoly acids, and metal oxides, respectively [27, 30-31]. However, to the best of my knowledge, the hydrogenation of algal biomass over a heterogeneous catalyst for the production of sugar alcohols has never been investigated, despite the advantageous features and the well-known cellulose-like structure as mentioned earlier.

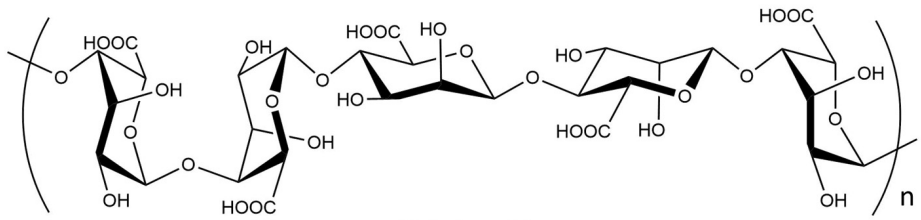

Alginic acid

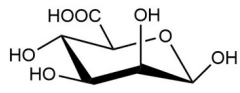

Mannuronic acid
(M)

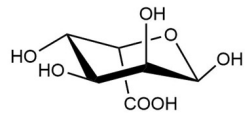

Guluronic acid
(G)

Scheme 1-3. Structure of alginic acid.

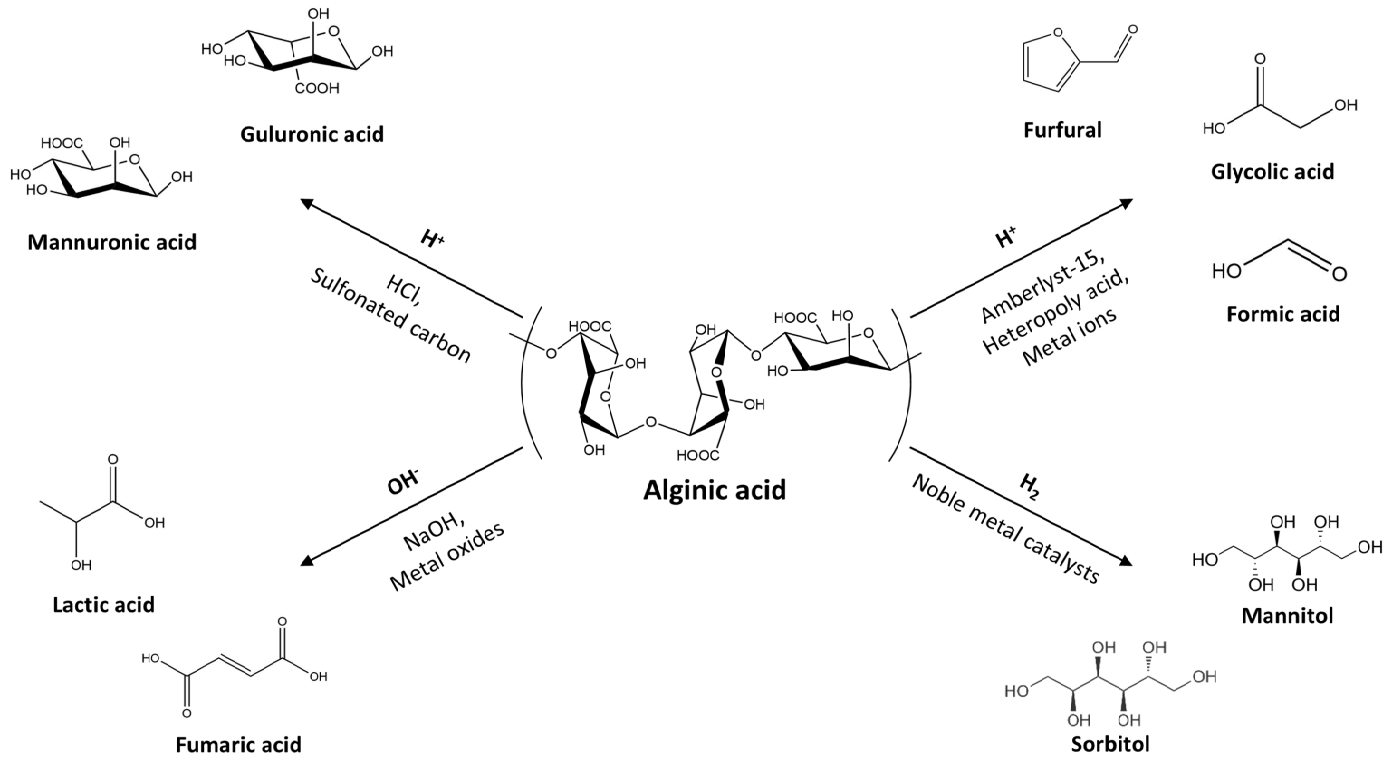

Scheme 1-4. Catalytic conversion of alginic acid into value-added platform chemicals.

1.4. Objective

In contrast to a wide range of researches on hydrogenation of cellulose, there still is a paucity of study on hydrogenation of alginic acid despite structural similarity between alginic acid and cellulose as mentioned earlier. In other words, the production of value-added renewable chemicals still heavily depends on lignocellulosic biomass, in spite of the various advantages of algal biomass over its terrestrial counterparts. Furthermore, the valorization of alginic acid is still confined to hydrolysis via acid catalysis only for the production of organic acids and furfural. Hence, in view of the need for a sustainable and green chemistry to diversify renewable feedstocks and the range of biomass-derived products, the direct hydrogenation of alginic acid over a solid catalyst into sugar alcohols is of great importance.

In this respect, the objective of this thesis is to investigate the hydrogenation of alginic acid into sorbitol and mannitol over Ru-based carbon catalysts. Various analytical techniques were applied to better elucidate a reaction pathway of the formation of the C6 sugar alcohols from alginic acid. In addition, different Ru-based catalysts were synthesized and employed to the reaction. The catalysts were thoroughly characterized to better understand the role of the catalysts in the reaction.

It is believed that the present research would suggest the potential of alginic acid as a promising surrogate for cellulose to produce sugar alcohols in combination with Ru-based heterogeneous catalysts. This will draw attention of fellow researchers into the field of catalytic utilization of alginic acid and reveal new insight to alleviate the current heavy dependence on lignocellulosic biomass for the production of green chemicals.

Chapter 2. Catalytic Hydrogenation of Alginic Acid into Sugar Alcohols over Noble Metal Supported on Carbon Catalysts

2.1. Introduction

In recent years, algal biomass, known as the third-generation biomass, has been attracting considerable attention as a promising renewable resource since it has more advantageous features than its terrestrial counterpart, cellulose, with respect to rapid growth, inedibility, and lignin-free composition. Marine biomass has been utilized in biorefinery processes such as liquefaction, pyrolysis, and gasification to produce value-added renewable chemicals, contributing to alleviate the heavy dependence on petroleum-based chemicals [34]. Recently, attempts have been made to produce value-added chemicals from alginic acid, a major constituent of macroalgae, via thermochemical methods. As already shown in Scheme 1-3, alginic acid consists of two different uronic acids, mannuronic acid (M) and guluronic acid (G) linked by β-1,4-glycosidic bond, which is analogous to the structure of cellulose composed of glucoses also linked by the ether bond. Recent studies reported that versatile platform chemicals such as uronic acids, lactic acid, and furfural could be produced from alginic acid via catalytic hydrothermal treatment [27-33]. However, to the best of my knowledge, catalytic hydrogenation of alginic acid into sugar alcohols over metal catalysts has never been studied systematically. Scheme 2-1 shows a comparison of the structure between cellulose and alginic acid, and their conversion to sugar

alcohols. Unlike the case for cellulose hydrogenation, additional hydrogenation steps are required for the production of sugar alcohols from alginic acid due to the presence of carboxylic groups. In addition, mannitol is produced along with sorbitol since alginic acid consists of two epimeric monomers (see Scheme 2-2 for a detailed reaction network).

In this chapter, macroalgae-derived alginic acid as a green alternative to cellulose was hydrogenated into sugar alcohols, mainly sorbitol and mannitol, over heterogeneous catalysts. A screening of noble metals, kinetic study, isomerization of hexitols, and durability test of the catalyst were performed. Based on results obtained from LC- and GC-MS, a plausible reaction network for the hydrogenation of alginic acid would then be proposed for the first time.

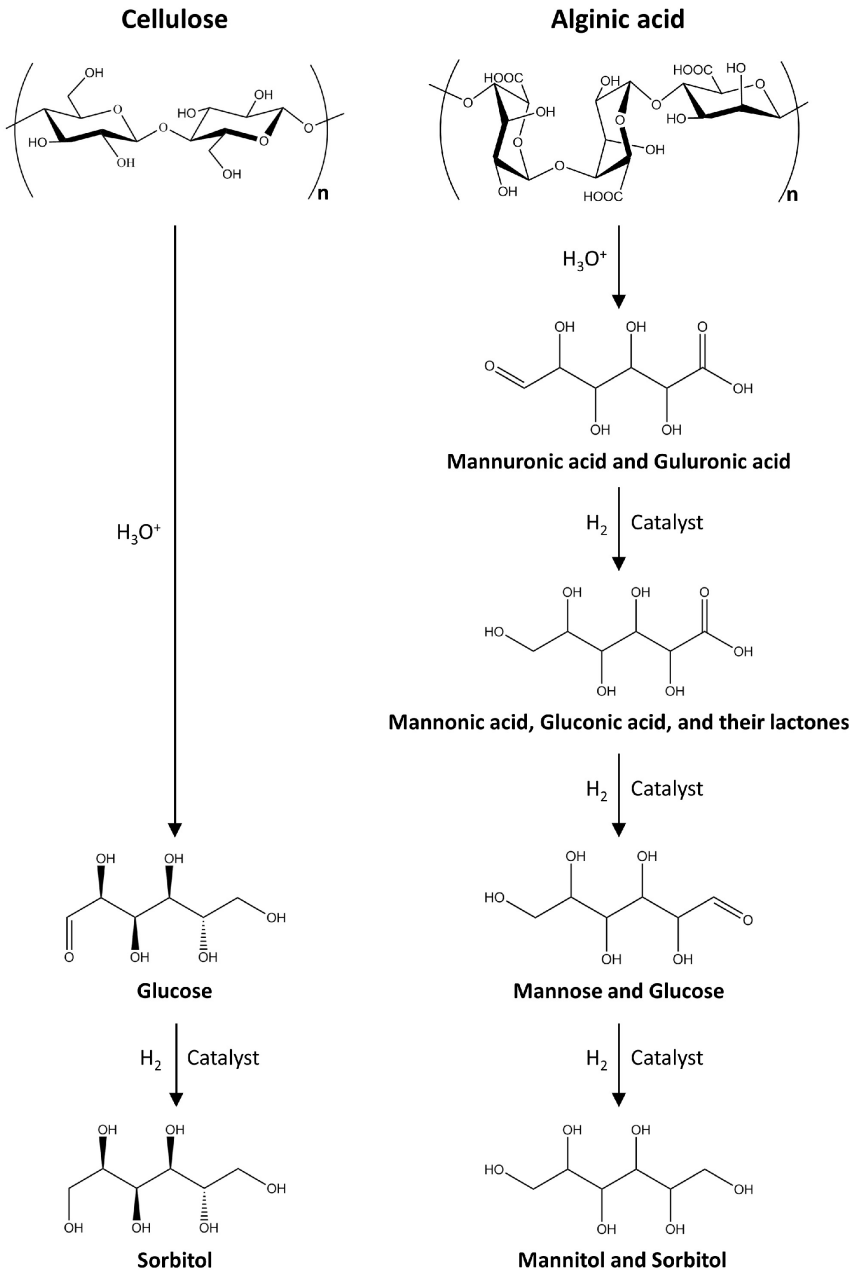

Scheme 2-1. Schematic reaction paths of sugar alcohol production via hydrogenation of cellulose and alginic acid.

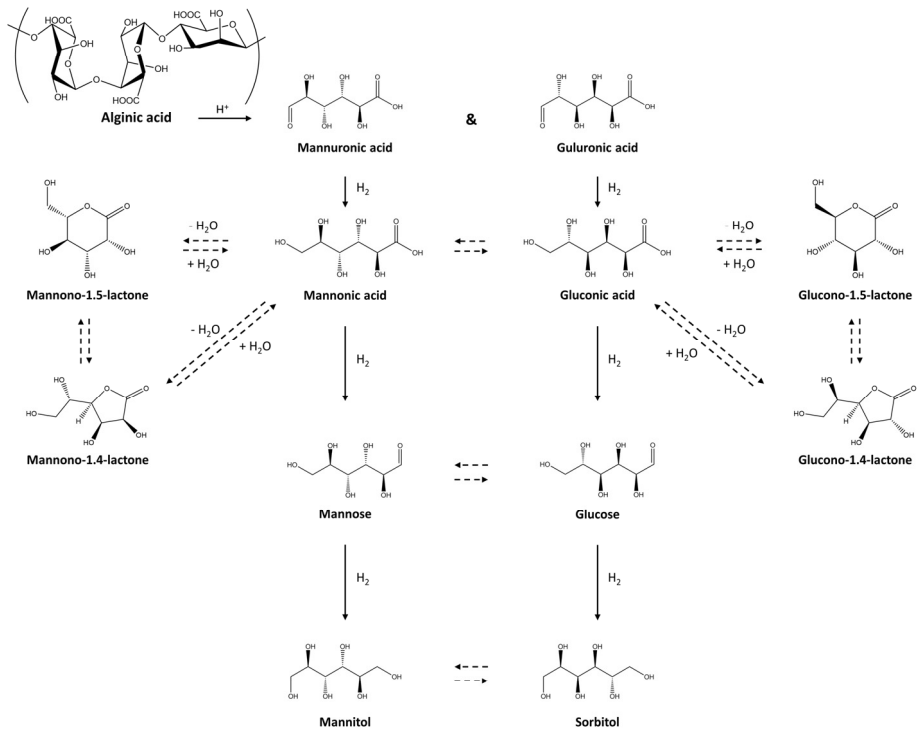

Scheme 2-2. A detailed reaction pathway of hydrogenation of alginic acid.

2.2. Experimental

2.2.1. Materials

Alginic acid and gluconic acid were purchased from Sigma-Aldrich. Mannuronic acid and guluronic acid were obtained from Qingda BZ Biotech. Sorbitol, mannitol, galactitol, arabitol, ribitol, xylitol, glycerol, propylene glycol, gluconolactone, mannose, and glucose were purchased from Alfa Aesar. Mannonolactone was obtained from TCI Chemicals. The above reagents were used as received. Activated carbon was purchased from Sigma-Aldrich. Commercial catalysts, Ru(5)/C, Pd(5)/C, Pt(5)/C, Rh(5)/C, and Ir(1)/C, were purchased from Alfa Aesar and used without further pretreatment. The commercial catalysts were denoted as M(x)/C(Alfa), where M and x refers to noble metal supported and loading amount of each metal (wt%), respectively.

2.2.2. Catalyst preparation

Activated carbon was partially oxidized with nitric acid of different concentrations to impart different amount of acid functionality. Typically, activated carbon was mixed with nitric acid with a volume to mass ratio of 10, varying the concentration of nitric acid. After 3 h at 110 °C, the resultant carbon was retrieved by filtration, washed with distilled water until the filtrate became neutral, and then oven-dried at 100 °C overnight. The oxidized activated carbons thus obtained were denoted as AC-N-x, where x represents concentration of nitric acid. 5 wt% of ruthenium was impregnated on the above activated carbons by conventional wet

impregnation method. Ru supported on nitric acid-treated activated carbon was reduced at 400 °C for 2 h under 10% H_2 flow (50 ccm) before being used in the reaction. The resultant Ru-based carbon catalysts were denoted as Ru(5)/AC-N-x, where x represents the molar concentration of nitric acid.

2.2.3. Catalyst characterization

The specific surface area of the catalysts was determined by Brunauer-Emmett-Teller (BET) method on Micromeritics ASAP 2010. The samples were degassed at 250 °C for at least 4 h before the analysis at -196 °C. FT-IR spectra of the catalysts were measured on Agilent Cary 660 with resolution of 4 cm^{-1} using KBr pellets which contain 5 wt% of a catalyst. CO chemisorption was performed on BEL-Cat (BEL JAPAN Inc.) to determine crystallite sizes and dispersions of ruthenium on catalysts. Typically, a sample was pre-reduced at 350 °C for 2 h under 5% H_2 flow (50 ccm). After the sample was cooled to the measurement temperature, 50 °C, under He flow (50 ccm), a CO pulse (4.98% CO/He, loop volume of 0.8570 cm^3) was introduced until the saturated coverage was obtained. The acid density of the catalysts was analyzed by back titration using 0.01 M of NaOH solution and 0.02 M of HCl solution with a drop of phenolphthalein solution.

2.2.4. Catalytic reaction

A typical reaction procedure is as follows: hydrolytic hydrogenation was performed in a stainless-steel autoclave with an inner volume of 100 mL charged with 0.3 g of alginic acid, 30 mL of distilled water, and the proper amount of catalyst.

The mass ratio of the reactant to metal was 105. Air in the reactor was removed by flushing the reactor with 50 bar of helium three times and the reactor was then pressurized with 50 bar of hydrogen. The reactor was heated to the desired temperature within 30 min in an electric furnace. The reaction mixture was agitated by a mechanical impeller at 1000 rpm during the reaction. After the desired reaction time, the reactor was quenched with ice-cold water within 10 min to prevent further reaction.

To evaluate the recyclability of the catalyst, a multi-batch procedure was designed to compensate a weight loss, which frequently occurs during the catalyst recovery. Briefly, four identical batch reactions were performed as described above. After each reaction, spent catalysts were retrieved via filtration and washed with distilled water and acetone, and dried in an oven at 100 °C. The spent catalysts were reused for the second run in three identical reactors and recovered again after the reaction for the next run. The same procedure was repeated for the third and fourth run.

Liquid products were analyzed by LC-MS, GC-MS, GPC, TOC, and ICP as described below.

2.2.5. Analytical methods

Gel permeation chromatography (GPC) was conducted on Ultimate 3000 (Dionex) equipped with a refractive index detector and a series of three columns (Waters Ultrahydrogel 120, 150, and 1000) maintained at 40 °C. 0.1 M of sodium azide solution as a mobile phase was eluted at a flow rate of 1.0 mL/min. The instrument was calibrated with Pullulan having a molecular weight distribution of

342-80500. The amount of Ru leached from the catalyst was measured by inductively coupled plasma-atomic emission spectroscopy (ICP-AES, PerkinElmer/Optima-4300 DV). The total organic carbon was measured using Sievers 5310 (GE) with an autosampler. Liquid chromatography-mass spectrometry (LC-MS) was performed on LCQ Deca XP Plus (Thermo Finnigan) equipped with an electrospray ionization module working in a positive mode. The liquid sample was infused into the equipment with 0.1% formate buffer. The values of m/z are 23 higher than the actual molecular weight of molecules due to the formation of sodium adduct during the analysis. The qualification of reaction products was conducted using gas chromatography-mass spectrometry (GC-MS) equipped with a DB-5MS column (60 m × 0.25 mm × 0.25 μm). Since the resolution of GC for the separation of various sugar alcohols is superior to that of liquid chromatography, the quantification of products was performed on GC equipped with a DB-5 column (60 m × 0.25 mm × 0.25 μm). Before injection to GC, the liquid aliquot was silylated according to the method previously reported [35]. The carbon-based yield was calculated as follows:

Carbon yield (%) = 100 × (number of carbon atoms in an organic compounds/6) × (moles of an organic compound in the product obtained by GC/moles of a repeating unit in alginic acid)

The composition of alginic acid, i.e. the ratio of mannuronic acid (M) to guluronic acid (G), was measured by ^{13}C nuclear magnetic resonance (^{13}C NMR) analysis referring to previous studies. The NMR spectrum was recorded using an NMR spectrometer (Bruker Avance II, 500 MHz) with a 4–mm probehead with a spectrometer frequency and spinning rate of 125.7 MHz and 5 kHz, respectively.

The ratio M/G was calculated by using the areas of designated peaks shown in Figure 2-1 as expressed in the following equation [36-37]:

$$M/G = (\text{Area E} + \text{Area F})/(\text{Area D} + \text{Area G} + \text{Area H})$$

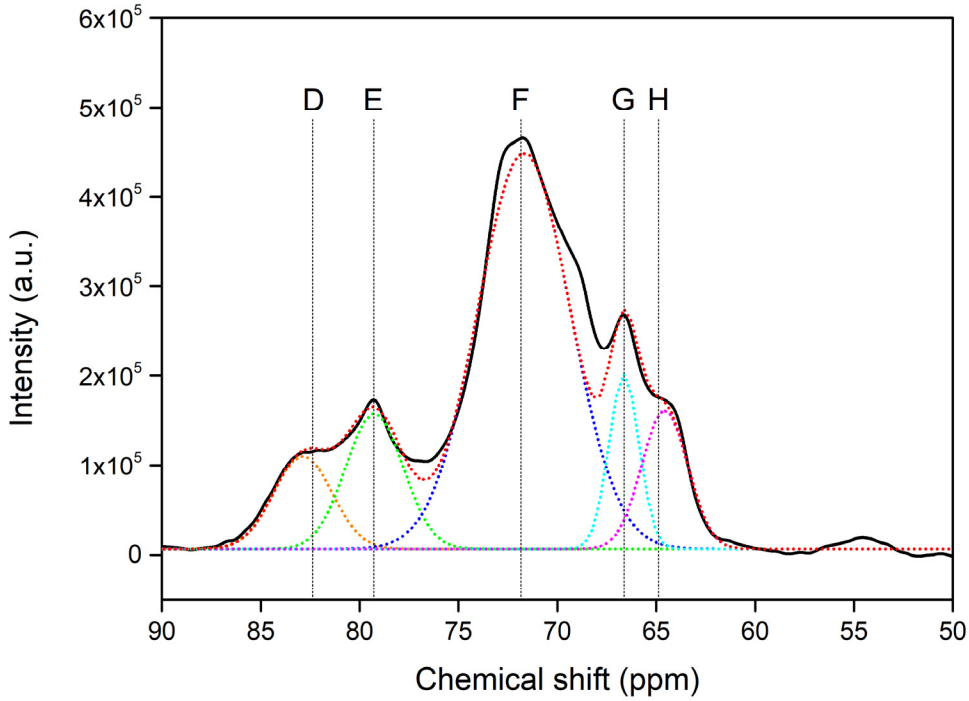

Figure 2-1. ^{13}C NMR spectrum of the reactant, alginic acid.

2.3. Results and discussion

2.3.1. Catalytic hydrogenation of alginic acid

The batch-wise hydrolytic hydrogenation was performed over various carbon-supported noble metals to produce sugar alcohols from alginic acid. As shown in Figure 2-2, the highest yield of C6 sugar alcohol (61%) was obtained over Ru, whereas carbon-supported Pd, Pt, Rh, and Ir catalysts hardly produced any C6 sugar alcohols although the complete conversion of alginic acid over the noble metal supported on carbon was observed by GPC analysis (Figure 2-3). This resulted in a significant loss in carbon balance for the Pd, Pt, Rh, and Ir supported catalysts. However, as summarized in Table 2-1, TOC analysis revealed that most of organic carbons (> 80%) were preserved in the liquid products, indicating that carbon loss to gas phase could be regarded as marginal. In other words, several byproducts were produced during the catalytic hydrogenation of alginic acid. It is known that different metals show different selectivities towards hydrogenation, C-C cleavage, and C-O cleavage. For example, a reaction of glycerol over ruthenium resulted in the formation of a fully hydrogenated product, propane [38], or a C-C cleaved product, ethylene glycol [39]. However, the production of a C-O cleaved product, propylene glycol, was favored over platinum [40]. This was evidenced by the detection of dideoxy-aldonic acid and dideoxy-aldonic acid lactones by GC-MS only for the cases of carbon-supported Pd, Pt, Rh, and Ir (data not shown). This was further analyzed by LC-MS and the result indicates a distinctive difference between carbon-supported Ru and the other noble metals as shown in Figure 2-4. Dideoxy-aldonic acid lactone (m/z=169.05) was observed for carbon-supported Pd, Pt, Rh, and Ir

catalysts while C6 sugar alcohols (m/z=205.08) were produced only for Ru(5)/C(Alfa). Thus, the cause of carbon loss could be attributed to the formation of byproducts via the hydrodeoxygenation of aldonic acid or its lactone over Pd, Pt, Rh, and Ir supported catalysts. Furthermore, unidentified compounds having low m/z were also produced over Pd, Pt, Rh, and Ir supported catalysts. Unfortunately, the quantification of these byproducts was not possible due to the absence of standard samples. The activity of the commercial catalyst, Ru(5)/C(Alfa) was also compared to that of activated carbon-supported Ru catalysts synthesized in-house. In the preparation of the Ru catalysts, activated carbon was oxidized with nitric acid of different concentrations to vary its acid density. Textural properties of the synthesized catalysts (Ru/AC-N-x) are listed in Table 2-2. As displayed in Figure 2-2, among Ru/AC-N-x catalysts, a catalyst oxidized with higher concentration of HNO_3 exhibited a higher yield of sugar alcohols. The result suggests that oxygenate functional groups such as phenolic OH, =O, and –COOH which were induced after nitric acid treatment have a promotional effect on the hydrolysis of alginic acid. Especially, amounts of weak acid site, carboxylic group, was obviously formed after the modification as evidenced by the evolution of C=O stretching vibration band at 1718 cm^{-1} (Figure 2-5) [41-42]. Similarly, the capability of carboxylic group to effectively hydrolyze biomass feedstock was reported both in cellulose and alginate valorization [30, 43]. However, the commercial Ru(5)/C (Alfa) catalyst having lower acid density exhibited higher activity towards the production of C6 sugar alcohols. The result implies that a metal site could also act as an effective acid site to hydrolyze alginic acid under pressurized H_2 atmosphere without any acid site. Therefore, it can be deduced that protonic acid sites formed by spilled-over hydrogen on ruthenium

could hydrolyze alginic acid effectively as in the case of hydrolytic hydrogenation of cellulose on Pt [44]. In addition, the role of ruthenium as an acid site was verified in hydrolysis of oligosaccharides into glucose [13]. The higher yields of sugar alcohols over the commercial catalyst can also be explained by the highest dispersion and the smallest size of Ru as listed in Table 2-3. As the effect of the crystallite size of Ru has already been determined, smaller Ru favored the formation of hydrogenated intermediate of cellobiose [45] and exhibited higher TOF on hydrogenation of glucose [46]. Hence, the crystallite size of Ru in addition to the acidity of the catalyst should be taken into account for the conversion of alginic acid into sugar alcohols. The loss in carbon yield for ruthenium supported carbon catalysts were ascribed mainly to byproducts such as n-deoxy hexitols and pentitols, and to few C_2-C_4 sugar alcohols as analyzed by GC-MS (data not shown). The short chain sugar alcohols (C_2-C_4) accounted for less than 2%. Unfortunately, the quantification of the other byproducts could not be realized due to the absence of authentic samples.

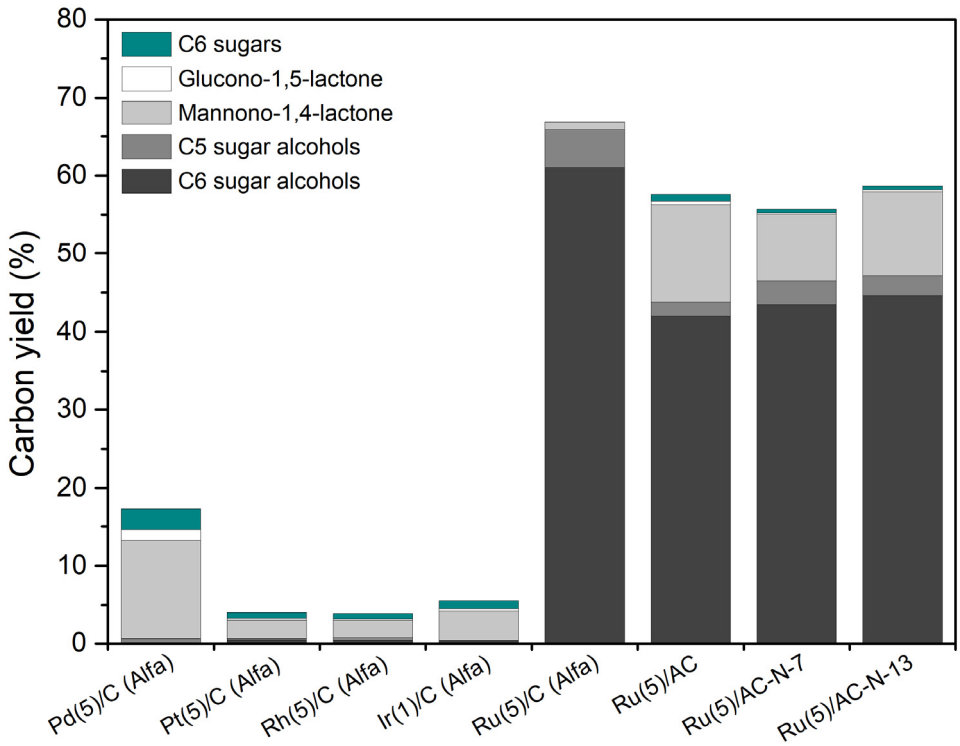

Figure 2-2. Product distribution over different carbon-supported noble metals at 150 °C for 12 h under 50 bar of H_2. C6 sugar alcohols: sorbitol, mannitol, and galactitol; C5 sugar alcohols: xylitol, arabitol, and ribitol; C6 sugars: glucose and mannose.

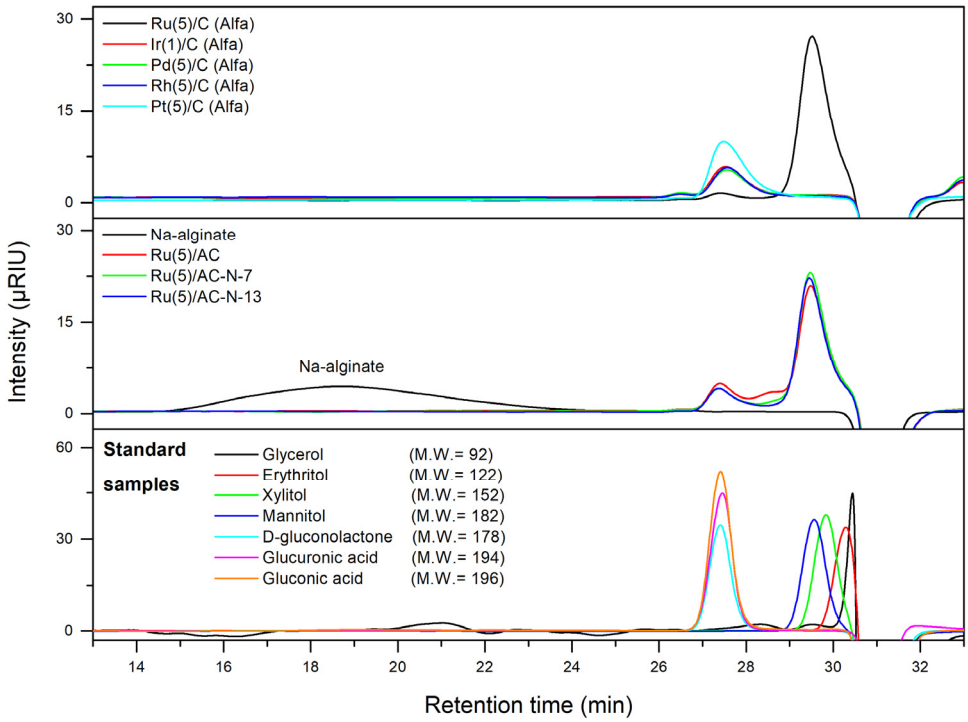

Figure 2-3. GPC chromatograms of products hydrogenated over carbon-supported noble metals at 150 °C for 12 h under 50 bar of H_2.

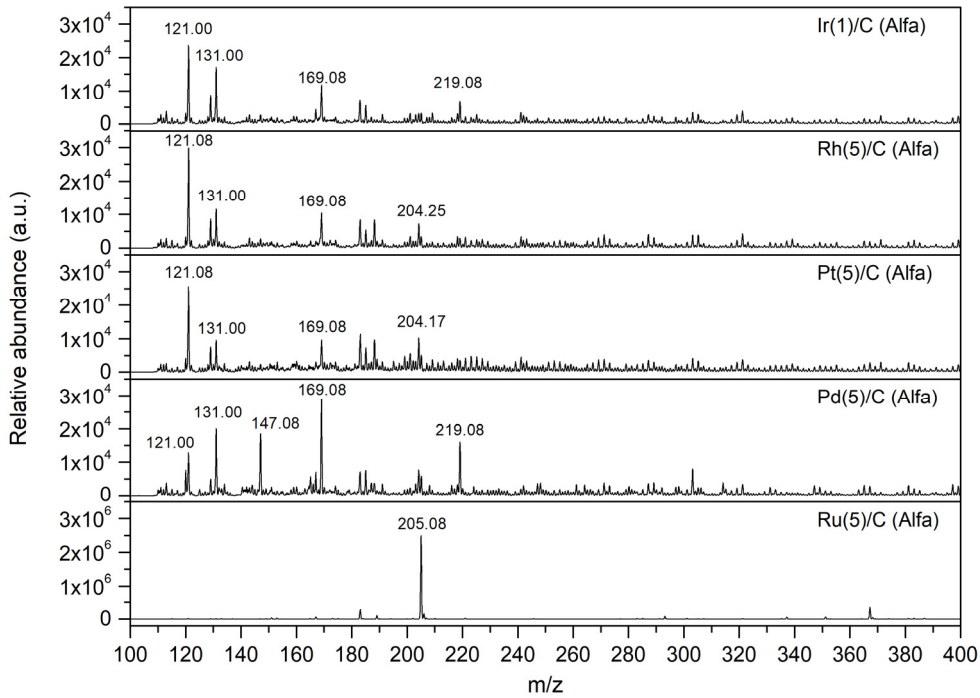

Figure 2-4. LC-MS spectra of products hydrogenated over carbon-supported noble metals at 150 °C for 12 h under 50 bar of H_2.

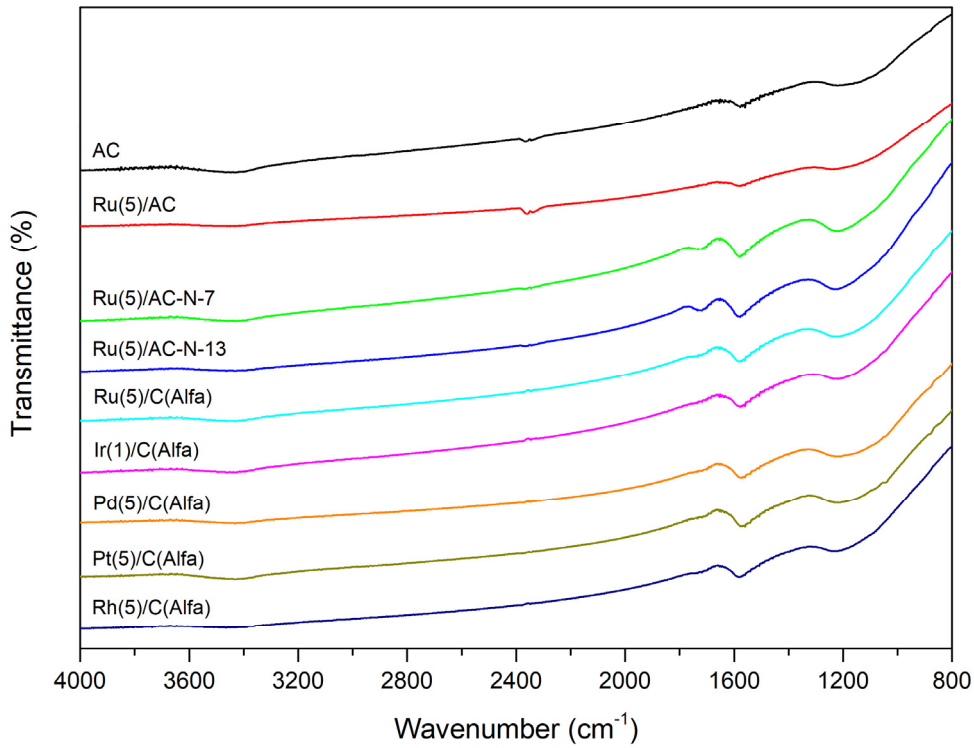

Figure 2-5. FT-IR spectra of commercial and in-house synthesized catalysts.

Table 2-1. Total organic carbon in liquid products after hydrogenation at 150 °C for 12 h under 50 bar of H_2.

Catalyst	Total organic carbon remained in liquid product (mg/L)	Total organic carbon remained in liquid product [a] (%)
Ru(5)/C (Alfa)	17.4	99.4
Pd(5)/C (Alfa)	19.0	108.6
Pt(5)/C (Alfa)	15.6	89.1
Rh(5)/C (Alfa)	17.2	98.3
Ir(1)/C (Alfa)	14.5	82.9

[a] The values were calculated based on total organic carbon of 1% alginic acid solution (17.5 mg/L)

Table 2-2. Textural properties of catalysts.

Catalyst	Surface area (m^2/g catalyst) [a]	Total acid density (mmol/g catalyst) [b]
Ru(5)/C (Alfa)	816.2	0.85
Pd(5)/C (Alfa)	810.5	0.51
Pt(5)/C (Alfa)	886.7	0.43
Rh(5)/C (Alfa)	872.5	0.62
Ir(5)/C (Alfa)	1017.5	0.43
Ru(5)/AC	941.8	0.26
Ru(5)/AC-N-7	894.0	1.11
Ru(5)/AC-N-13	824.7	1.11

[a] Surface area was measured by Brunauer-Emmet-Teller method.

[b] Total acid density was determined by back titration.

Table 2-3 . Dispersions and crystallite sizes of ruthenium on different carbons.

Catalyst	Dispersion [a] (%)	Crystallite size [b] (nm)	Yield $_{C6\ sugar\ alcohols}$ [c] (%)
Ru(5)/C (Alfa)	36	3.7	61.0
Ru(5)/AC	26	5.1	42.0
Ru(5)/AC-N-7	27	4.9	43.5
Ru(5)/AC-N-13	17	7.9	44.6

[a] Dispersion was determined by CO chemisorption.

[b] Crystallite size of ruthenium was measured by CO chemisorption.

[c] Alginic acid was hydrogenated at 150 °C for 12 h under 50 bar of H_2.

2.3.2. Stability of the commercial Ru catalyst

Regarding a practical application of heterogeneous catalysts, durability of catalysts is of great importance. To check the recyclability of the catalyst, Ru(5)/C(Alfa), in this reaction system, several identical batch reactions were performed, and liquid aliquots and the spent catalyst were analyzed. As shown in Figure 2-6, ruthenium was leached from the catalyst after repeated reactions. The decrease of the yield of C6 sugar alcohols is in line with the decrease in the amount of residual ruthenium over repeated reactions. Furthermore, as listed in Table 2-4, the CO chemisorption result shows that dispersion of Ru on carbon decreased from 36% to 11% along with the increase in crystallite size of the metal from 3.7 nm to 12.2 nm after the 4th recycle run. Thus, the deactivation of the catalyst could be ascribed to the aggregation of ruthenium as well as to the leaching of the metal. In addition, Durability of the catalyst in a concentrated alginic acid solution was also examined since an industrial conversion of biomass occurs mostly in bulk. As listed in Table 2-5, the leaching of ruthenium was accelerated in concentrated solutions of alginic acid. Ruthenium was leached gradually from 0.5 to 2.40% in alginic acid solutions of concentration below 10%. However, a sharp leaching of Ru was observed in the reactant concentration of 30%. The reason for the intense leaching might lie in the acidic nature of the reactant, alginic acid, which can behave as a ligand to form a metal-alginic acid complex [47-49].

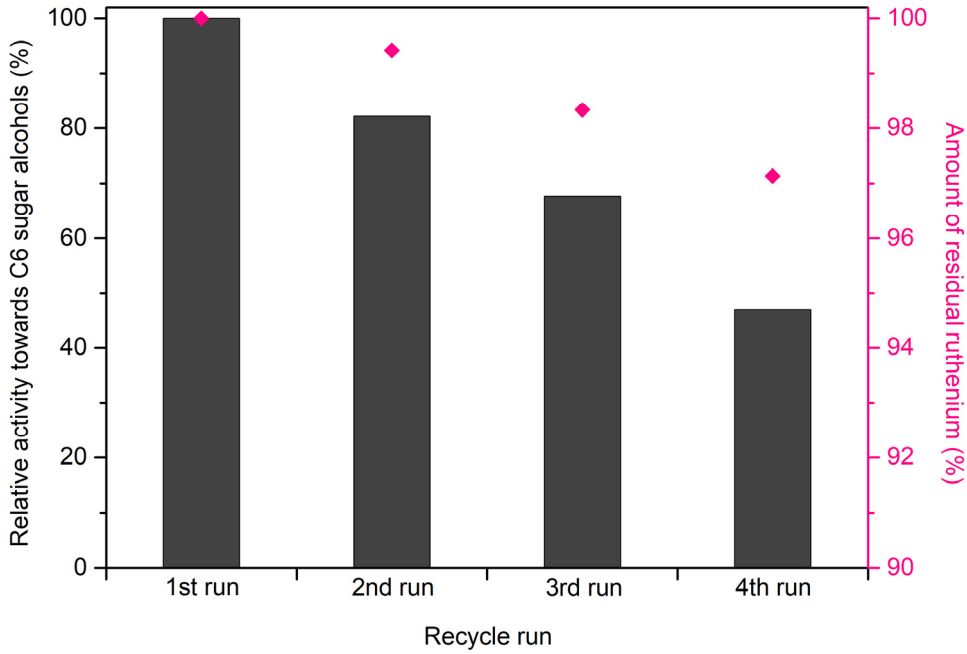

Figure 2-6. Recycling of Ru(5)/C(Alfa) at 180 °C for 2 h under 50 bar of H_2.

Table 2-4 . Dispersions and crystallite sizes of ruthenium after recycle reactions.[a]

Recycle Run	Dispersion [b] (%)	Crystallite size [b] (nm)
1st (Fresh catalyst)	36	3.7
2nd	29	4.6
3rd	19	6.9
4th	11	12.2

[a] The recycle reactions were performed at 180 °C for 2 h under 50 bar of H_2.

[b] Dispersion and crystallite size were measured by CO chemisorption.

Table 2-5. Amount of ruthenium leached after the hydrogenation in concentrated solutions of alginic acid.[a]

Alginic acid concentration [%(w/v)]	Ru leached [b] (%)	Residual Ru [c] (%)
1	0.58	99.4
5	1.85	98.2
10	2.40	97.6
30	9.28	90.7

[a] Reactions were performed at 150 °C for 12 h under 50 bar of H_2 over 0.1 g of Ru(5)/C(Alfa).

[b] The amount of Ru leached into the liquid was measured by ICP-AES.

[c] The values were calculated based on the amount of Ru on the fresh catalyst.

2.3.3. Reaction pathway of the hydrogenation of alginic acid

To investigate a plausible reaction pathway for the hydrogenation of alginic acid, kinetic studies were performed over Ru(5)/C(Alfa). Alginic acid was hydrolytically hydrogenated at 90 °C, and the resultant liquid products were then analyzed by LC-MS, as shown in Figure 2-7. It was observed that alginic acid was decomposed into chunks of oligomers ranging from dimer (m/z=393) to undecamer (m/z=1977) with a difference of 176 in m/z between neighboring peaks. At the early stage of the reaction, however, no sign of a peak corresponding to monomeric units (uronic acids, m/z=217) was observed. The above results suggest that the glycosidic bonds of alginic acid are cleaved in a random fashion; not in an ordered way releasing the outermost monomer unit one by one. As the reaction time was prolonged, aldonic acids (m/z=219) and sugar alcohols (m/z=205) started to be evolved along with the production of intermediates (m/z=377, 381, 393, 395) composed of two monomeric units. Unlike the case for the hydrolytic hydrogenation of cellobiose having one reducing aldehyde group where formation of only one intermediate, glucopyranosyl-glucitol, was observed [45], the additional carboxylic group on the monomeric unit of alginic acid caused the evolution of 5 different partially hydrogenated intermediates. From the result above, it could confidently be suggested that the formation of C6 sugar alcohols from alginic acid occurs through the consecutive hydrogenation of both aldehyde- or carboxyl-ends in oligomeric compounds, which is then followed by the cleavage of the glycosidic bonds between monomers of alginic acid to yield C6 sugar alcohols. A reaction pathway for the formation of sugar alcohols through these intermediates was proposed in Scheme 2-3. Furthermore, relative amounts of each intermediate are shown in Figure 2-8. Only a small amount

of aldonic acid (m/z=219) was produced, whereas the accumulation of intermediates composed of two monomeric units (m/z=381 and 395) was observed. This implies that the hydrolysis of the glycosidic bond would be a rate-determining step in the catalytic conversion of alginic acid to sugar alcohols. Similarly, the cleavage of the ether linkage between glucose in cellulose, viz. hydrolysis, was well-reported to be the rate-determining step in the hydrolytic hydrogenation of cellulose [50].

Since the difficulty lies in separating unreacted alginic acid from the catalyst and liquid products, conversion of alginic acid in this work was determined qualitatively by GPC analysis. As shown in Figure 2-9, the depolymerization of alginic acid over Ru(5)/C(Alfa) was promoted as the reaction time and temperature increased. At reaction temperatures higher than 90 °C, alginic acid was completely converted into smaller molecules within 1 h of reaction. The facile conversion of the biopolymer in the absence of any acid catalyst is due partly to the increase of ion product of water at elevated temperatures [51] and partly to the Brønsted acid formed in-situ from Ru on carbon under pressurized H_2 [44]. The effect of reaction time and temperature on the hydrolytic hydrogenation of alginic acid is quantitatively shown in Figure 2-10(a). As already shown in GPC analysis (Figure 2-9), the depolymerization of alginic acid proceeded tardily at low temperature, 90 °C, resulting in low yields of uronic acids (4.4%) and C6 sugar alcohols (3.2%) even after a prolonged reaction (48 h). The yield of C6 sugar alcohols increased sharply upon elevating the reaction temperature from 90 °C to 150 °C and the reaction time from 1 h to 12 h. The highest yield of C6 sugar alcohols, 61.0%, was obtained when alginic acid was hydrolytically hydrogenated at 150 °C for 12 h over Ru(5)/C(Alfa) under 50 bar of H_2. However, further increase in temperature to 210 °C reduced the yield of C6 sugar alcohol due

to the decomposition of C6 sugar alcohols into lower alcohols [18]. In the early stage of the reaction, it was observed that aldonic acid lactones and sugars were evolved first as intermediates and disappeared with the production of C6 sugar alcohols as shown in Figure 2-10(b). On the other hand, small amounts of uronic acids were observed, which again suggests that the consecutive hydrogenation of uronic acids into C6 sugar alcohols is faster than the hydrolysis of alginic acid into uronic acids.

The yields of individual C5 and C6 sugar alcohols are shown in Figure 2-10(c). It was observed that both sorbitol and mannitol were mainly produced from alginic acid over Ru(5)/C(Alfa). In fact, the production of mannitol is a distinctive feature of the hydrogenation of alginic acid since sorbitol is predominantly produced by the hydrolytic hydrogenation of cellulose over various metal supported catalysts [52]. The difference in the distribution of sugar alcohols is most likely attributed to the composition of alginic acid since G and M can be converted to sorbitol and mannitol, respectively. To further investigate the origin of mannitol, alginic acid was analyzed by ^{13}C NMR analysis (Figure 2-1). The ^{13}C NMR analysis revealed that the alginic acid used in this work is M-rich, representing a ratio of M/G of ca. 2.5. In this regard, mannitol should have been produced more abundantly than sorbitol. However, as shown in Figure 2-10(c), sorbitol was produced in larger quantities than mannitol under all the reaction conditions. Such discrepancy can be ascribed to two reasons: an isomerization of produced hexitols and different initial reaction rates of intermediates, aldonic acid lactones.

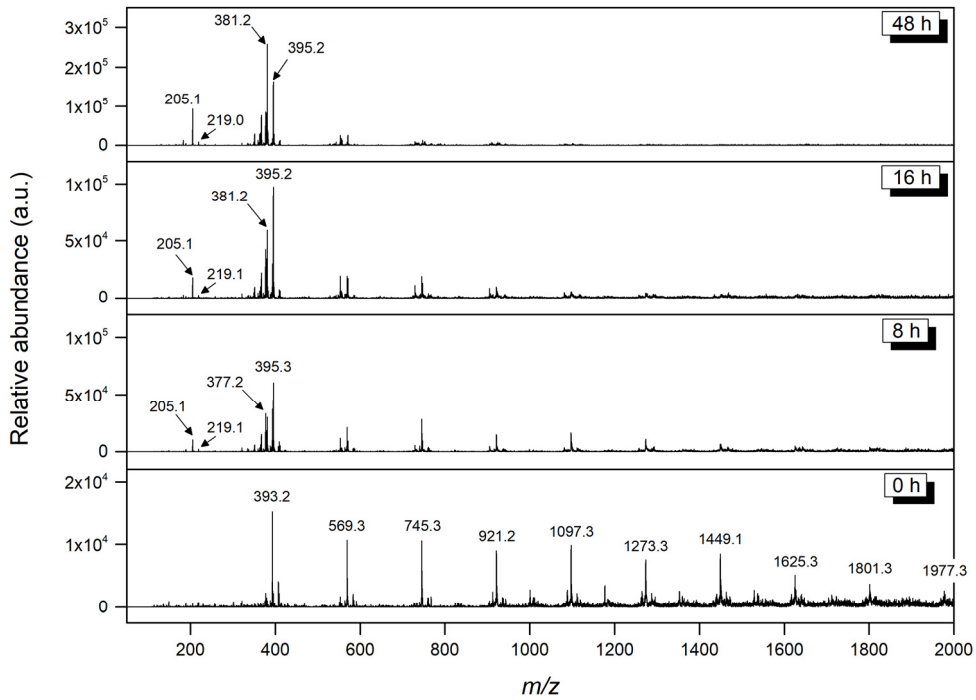

Figure 2-7. LC-MS spectra of products obtained at 90 °C under 50 bar of H_2 for different reaction times over Ru(5)/C(Alfa).

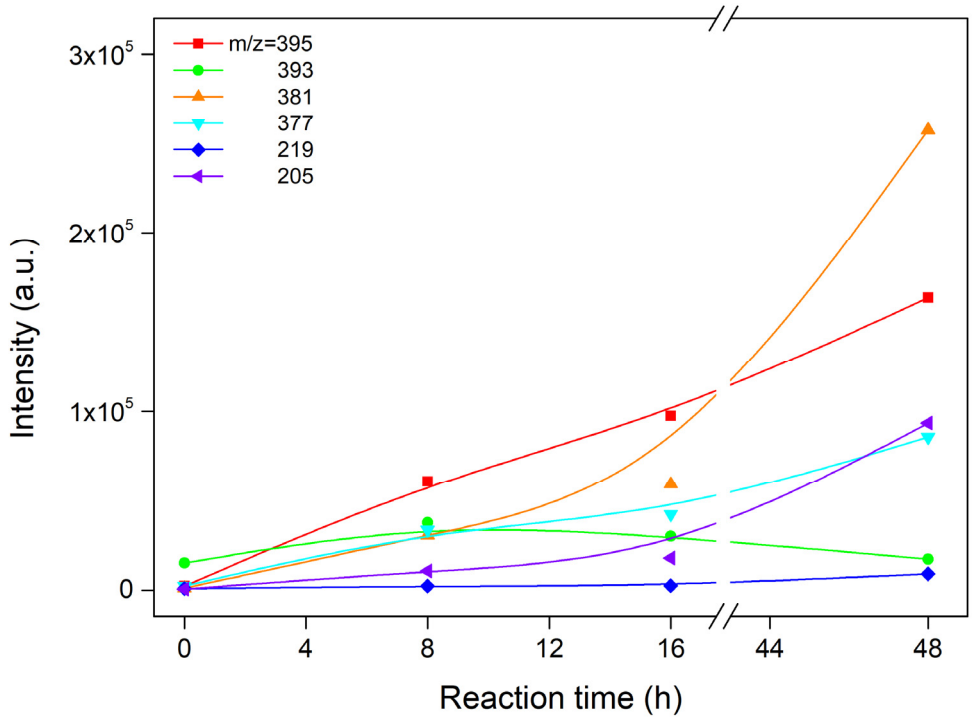

Figure 2-8. A time-course of evolution and reduction of intermediates at 90 °C over Ru(5)/C(Alfa) under 50 bar of H_2.

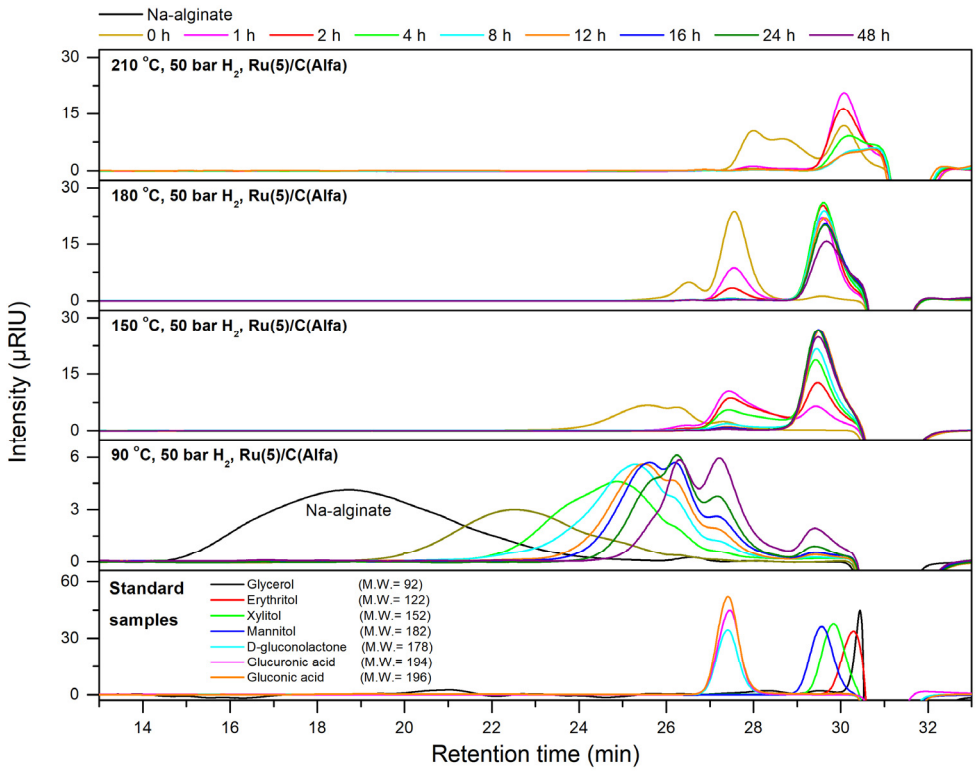

Figure 2-9. GPC chromatograms of products hydrogenated over Ru(5)/C(Alfa) at different reaction temperatures under 50 bar of H_2**.**

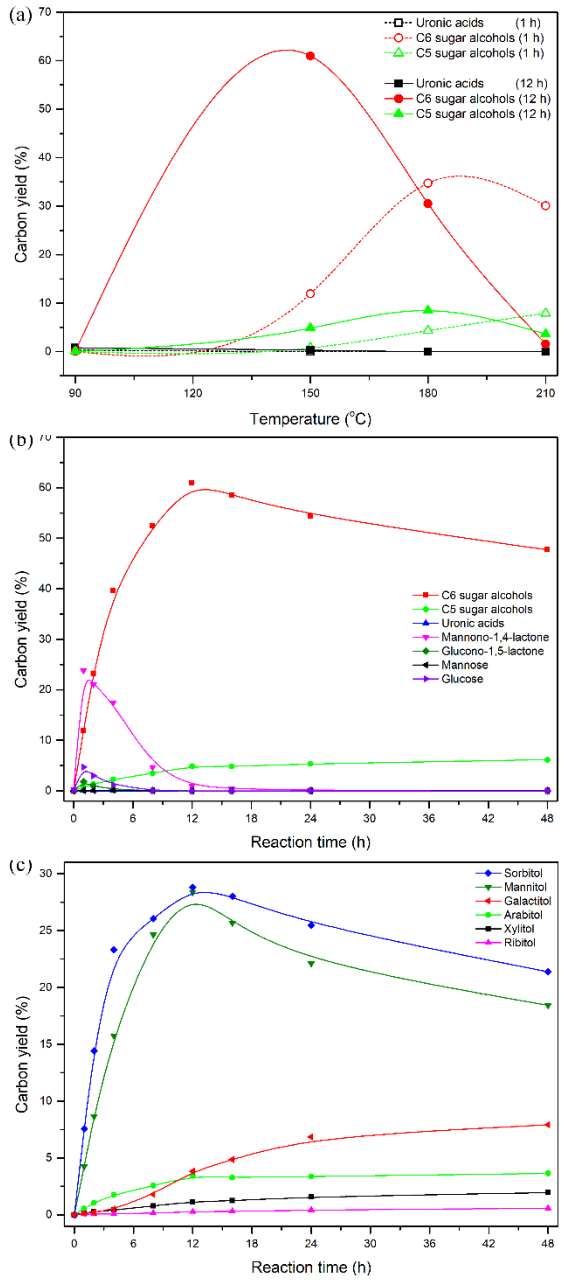

Figure 2-10. Yields of products as a function of reaction temperature (a), yield of products at 150 °C as a function of reaction time (b), and detailed sugar alcohol distribution at 150 °C as a function of reaction time (c) over Ru(5)/C(Alfa) under 50 bar of H_2.

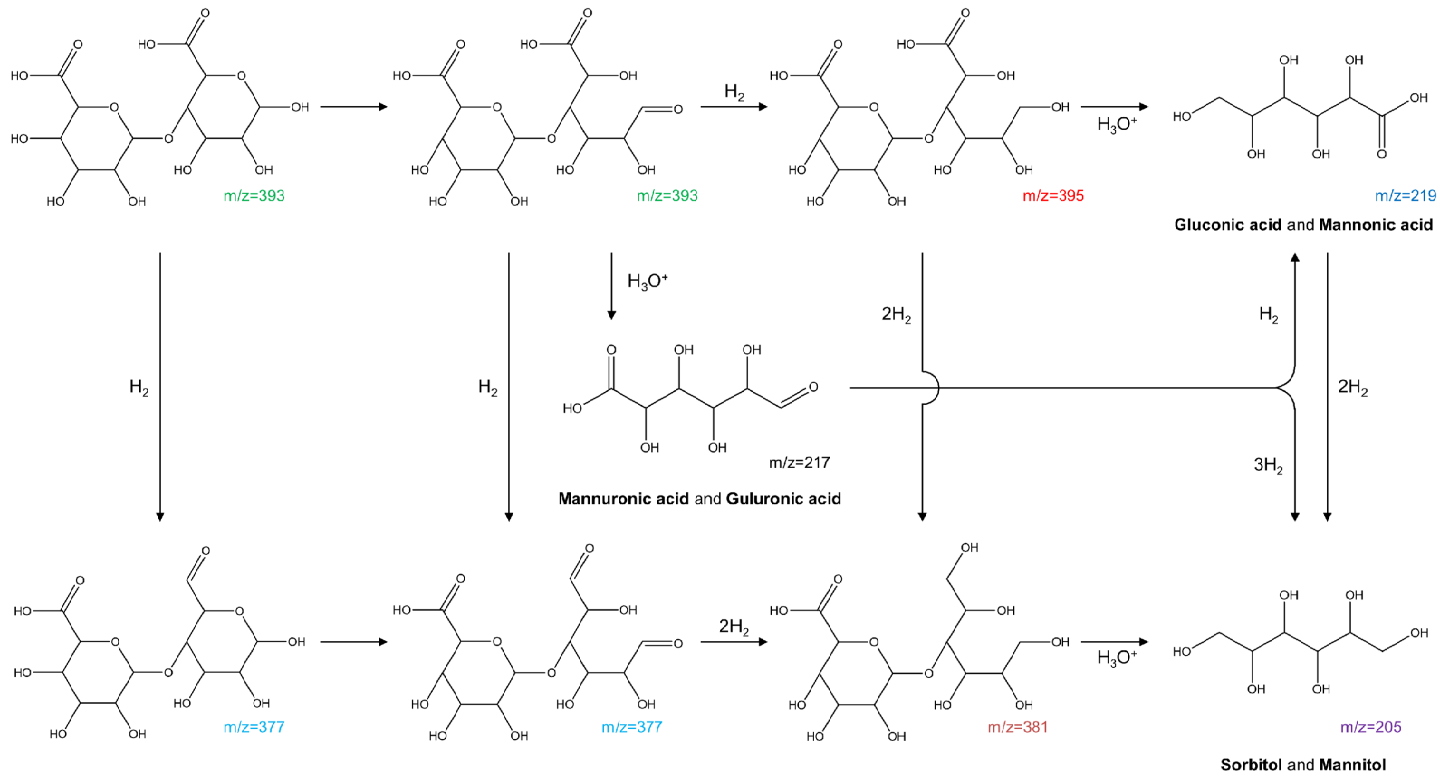

Scheme 2-3. A possible reaction scheme of hydrolytic hydrogenation of alginic acid oligomer.

2.3.4. Isomerization between produced sugar alcohols

The isomerization of sugar alcohols has been frequently observed during the hydrogenation of cellulose or glucose [18, 50, 52]. Sugar alcohols equilibrate with each other in the presence of H_2 [53] and the isomerization of sugar alcohols was found to be catalyzed by metal sites, resulting in different sorbitol to mannitol ratios under various catalytic systems [54]. For example, the ratio was reported to be ca. 4 over Pt/γ-Al_2O_3 during the hydrogenation of cellulose [44] and to be ca. 2 over Ru/C during the hydrogenolysis of sorbitol [54]. When alginic acid underwent hydrogenation in the present catalytic system, the ratio was found to be ca. 1.2 over Ru/C as shown in Figure 2-11(a). To further investigate the equilibrium between sugar alcohols, model reactions were conducted under the same reaction condition using sorbitol, mannitol, glucose, mannose, and lactones as a reactant. As shown in Figure 2-11(b), regardless of the reactants used, the ratios converged to ca. 1.3. Such value is in accordance with the ratio obtained from raw alginic acid.

However, at the early stage of hydrogenation of alginic acid, the ratio reached ca. 1.8. This could be attributed to the different initial hydrogenation rates of intermediates such as mannonolactone and gluconolactone. As seen from the initial slopes of aldonolactone hydrogenation in Figure 2-12, gluconolactone was hydrogenated 5-fold faster than mannonolactone from which sorbitol and mannitol were produced, respectively. Thus, the ratio of sorbitol to mannitol could be higher than the value from the equilibrium at the early stage of the reaction.

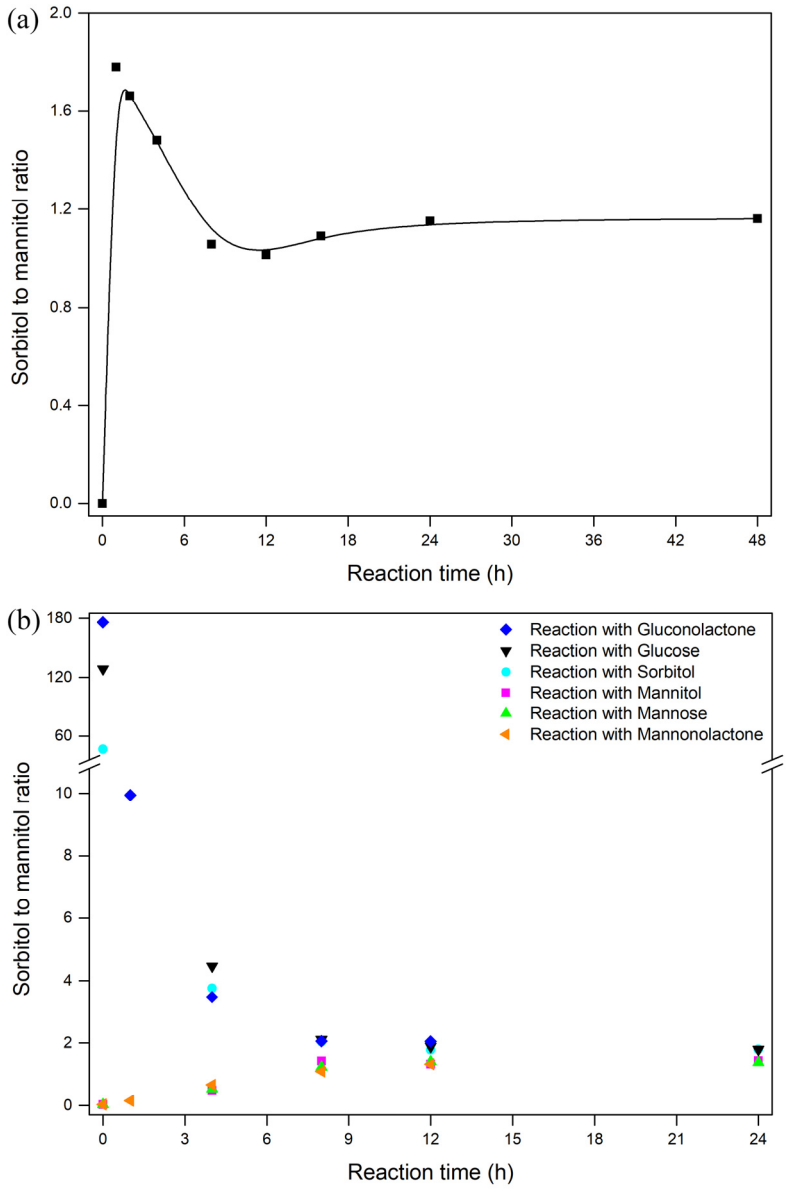

Figure 2-11. Time-course of sorbitol to mannitol ratio over Ru(5)/C(Alfa) during the hydrogenation of (a) alginic acid and (b) model molecules at 150 °C under 50 bar of H_2.

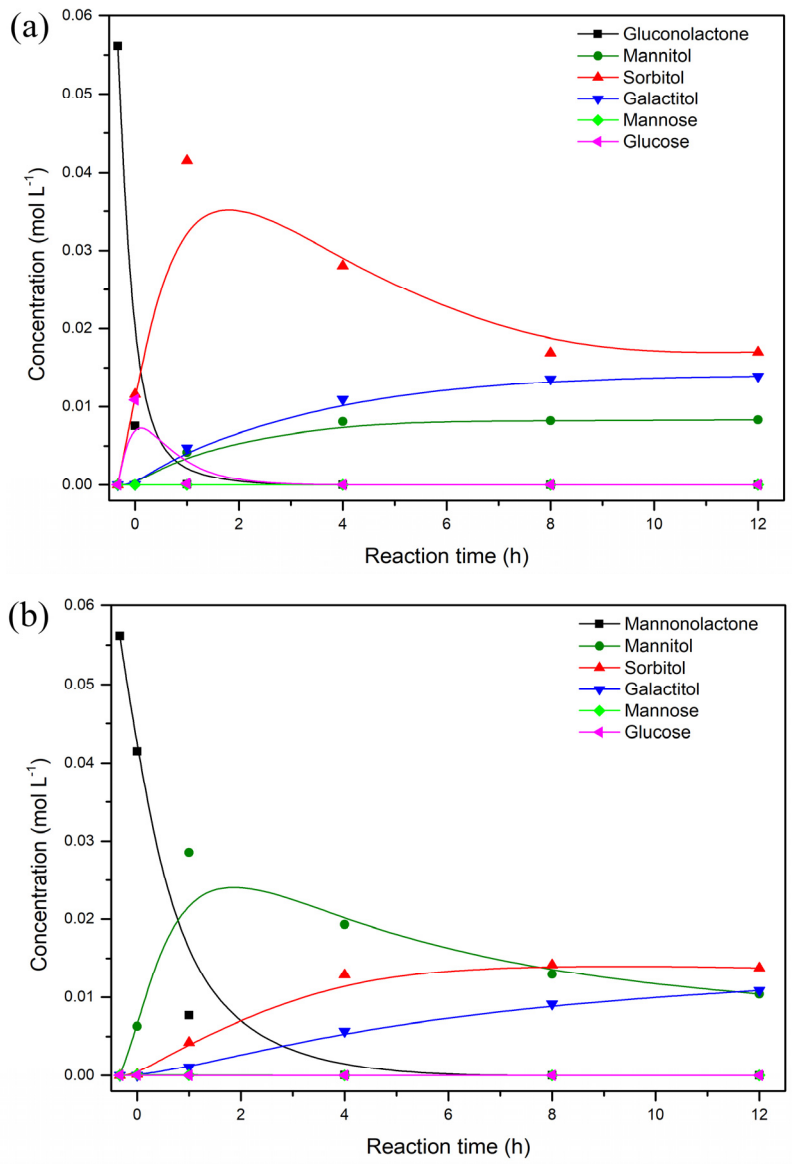

Figure 2-12. Concentrations of intermediates and products as a function of reaction time. (a) gluconolactone and (b) mannonolactone were hydrogenated over Ru(5)/C(Alfa) at 150 °C under 50 bar of H_2.

Chapter 3. Catalytic Hydrogenation of Alginic Acid into Sugar Alcohols over RuCu Bimetallic Catalysts

3.1. Introduction

In the previous chapter, alginic acid was successfully hydrogenated into C6 sugar alcohols over Ru supported on carbon catalysts. However, apart from sorbitol and mannitol, the formation of byproducts such as short chain sugar alcohols and galactitol via C-C cleavage and isomerization, respectively, was observed. In this regard, to enhance selectivity towards sorbitol and mannitol, various transition metal-promoted catalysts would be investigated in this chapter. Among various bimetallic catalysts studied, Cu-promoted catalyst exhibited superior catalytic activity compared to other bimetallic catalysts and monometallic catalysts.

It has been suggested that the interfacial interaction between Ru and Cu is the reason for unique catalytic properties of RuCu bimetallic catalysts, although these two metals are completely immiscible in bulk [55]. Addition of Cu to Ru catalysts has both geometric and electronic effects. It has been previously shown that the addition of the second metal can cause the formation of a thin layer of Cu on Ru kernel and electron transfer between Ru and Cu [56-57]. Due to above features and enhanced ability of hydrogen spillover, a RuCu bimetallic catalyst displays higher activity than monometallic catalysts in numerous fields of reactions. For instance, catalytic activity was enhanced by the addition of Cu to Ru-based catalyst in hydrogenation of glucose into sorbitol [58].

In the present chapter, RuCu bimetallic catalysts were applied to hydrogenation of alginic acid into C6 sugar alcohols for the first time. Electronic and geometric effects raised by the addition of Cu and the role of Cu in the hydrogenation reaction were elucidated by various characterization techniques.

3.2. Experimental

3.2.1. Materials

Activated carbon (AC) was purchased from Sigma-Aldrich. Nitric acid was supplied from Samchun Chemical Co., Ltd. Various metal precursors of $SnCl_4 \cdot 5H_2O$, $Fe(NO_3)_3 \cdot 9H_2O$, $Co(NO_3)_2 \cdot 6H_2O$, $(NH_4)_6Mo_7O_{24}$, and $Cu(NO_3)_2 \cdot 3H_2O$ were bought from Sigma-Aldrich except $RuCl_3 \cdot xH_2O$ and $Ni(NO_3)_2 \cdot 6H_2O$ from Alfa Aesar. Alginic acid was obtained from Sigma-Aldrich. Sugar alcohols (sorbitol, mannitol, galactitol, arabitol, ribitol, and xylitol), polyols (glycerol and propylene glycol), sugars (glucose and mannose), and glucono-1,5-lactone were purchased from Alfa Aesar. Mannono-1,4-lactone was supplied from TCI Chemicals. All chemicals were used without further purification.

3.2.2. Catalyst preparation

Ru-based bimetallic catalysts were synthesized via traditional wet impregnation method using aqueous solutions of metal precursors. Activated carbon was oxidized with 13 N of nitric acid to impart acidity according to the method reported elsewhere [30]. The nitric acid-treated carbon thus obtained was denoted as AC-N-13. Loading amount of Ru was maintained at 5 wt% while those of other promoters were kept at 1 wt%. Loading amount of Cu varied (1, 3, 5, and 10 wt%). Wet-impregnated catalysts were dried in an oven at 100 °C overnight followed by reduction at 300 °C for 3 h under 10% H_2 stream (100 ccm). Reduced catalysts were passivated under 5% O_2/N_2 (100 ccm) to prevent sudden oxidation upon exposure to air. Resultant

catalysts are denoted as Ru(5)M(x)/AC-N-13, where M and x stand for a promoter used and weight percent of the metal, respectively.

3.2.3. Catalyst characterization

N_2 adsorption-desorption analysis was performed on a BELSORP-mini II (BEL Japan Inc.). Catalysts were evacuated at 200 °C for at least 3 h before analysis. An X-ray diffractometer (Rigaku, CuKα radiation with 40 kV and 30 mA) was used to analyze diffraction patterns of catalysts. To investigate acid densities of catalysts, back titration was performed using NaOH (0.01 M) and HCl (0.02 M) according to a previously reported method.[30] To determine the amounts of Ru and Cu leached, inductively coupled plasma atomic emission spectroscopy (ICP-AES) was conducted on an Optima-4300DV (PerkinElmer). H_2 or CO chemisorption analysis was performed on a BELCat (BEL Japan Inc.). Before pulse chemisorption, a catalyst was reduced at 300 °C for 2 h under 5% H_2/Ar flow (50 ccm). After cooling down to 50 °C, a pulse of H_2 or CO was injected with loop volume of 0.8570 mL until saturated coverage was achieved. Temperature programmed reduction (H_2-TPR) of the catalyst was then executed on a BEL-CAT BASIC (BEL Japan Inc.). Prior to the detection of hydrogen uptake by a thermal conductivity detector, a catalyst was pretreated at 150 °C for 2 h under Ar stream (50 ccm). After cooling down to 40 °C, the sample was heated to 900 °C with a ramping rate of 10 °C/min under 5% H_2/Ar flow (50 ccm). X-ray absorption spectroscopy (XAS) was carried out on the 7D beamline of Pohang Light Source (PLS-II) with SR E-beam energy of 2.5 GeV and SR current of 360 mA using Si(111) crystal as a monochromator.

3.2.4. Catalytic hydrogenation reaction

Hydrogenation of alginic acid was carried out in an autoclave (100 mL, Parr Instrument Company). Alginic acid (0.3 g), distilled water (30 mL), and a catalyst (0.1 g) were charged into the autoclave. The vessel was heated to a desired reaction temperature under 50 bar of H_2 after purging with 50 bar of H_2 three times to remove air inside. After a desired reaction time, the reactor was quickly quenched in an ice-cold bath to avoid side reactions. The liquid mixture inside the vessel was agitated with an impeller at 1000 rpm during ramping and reaction. Recyclability experiment was performed using a multi-batch process according to a previously reported method to compensate weight loss of the catalyst during a catalyst recovery step [30].

3.2.5. Analytical methods

Gas chromatography (GC, Agilent 6890) equipped with a DB-5 column and an autosampler was utilized to analyze liquid products. Before injection to GC, liquid products were filtered and freeze-dried followed by silylation with BSTFA (N,O-Bis trimethylsilyl trifluoroacetamide) [59]. The carbon yield was calculated as below:

Carbon yield (%) = 100 × (number of carbon atoms in an organic compounds/6) × (moles of an organic compound in the product obtained by GC/moles of a repeating unit in alginic acid)

Total organic carbon (TOC) was measured by injecting the filtered liquid product into Sievers 5310C (GE). Gel permeation chromatography (GPC) was performed on Dionex Ultimate 3000 calibrated with Pullulan (molecular weight, 342-80500).

3.3. Results and discussion

3.3.1. Screening of Ru-based bimetallic catalysts

Various Ru-based bimetallic catalysts were synthesized and applied to hydrolytic hydrogenation of alginic acid for the production of sugar alcohols, mainly sorbitol and mannitol. The support material used was nitric acid-treated activated carbon to facilitate the hydrolysis of glycosidic bonds in alginic acid since the acidity of activated carbon could be enhanced by oxidation of carbon materials with nitric acid [60]. It has been previously reported that the acid density of various carbon materials is increased when the concentration of nitric acid is increased, resulting in improved hydrolysis of sodium alginate into uronic acids [30]. As shown in Figure 3-1, a screening experiment was carried out at 150 °C for 3 h. It was found that Cu-promoted catalyst exhibited the highest sugar alcohol ratio of C6/(C4+C5) and the lowest galactitol formation. The formation of byproducts such as C4-C5 sugar alcohols and galactitol would decrease the selectivity to desired products, namely sorbitol and mannitol. Thus, Cu was chosen for further studies shown below. Since the cleavage of C-C bonds and the isomerization of sugar alcohols could be expedited under harsher reaction condition, the reaction temperature was further elevated to 180 °C to better understand a synergistic effect of Cu addition on Ru catalyst [61-62].

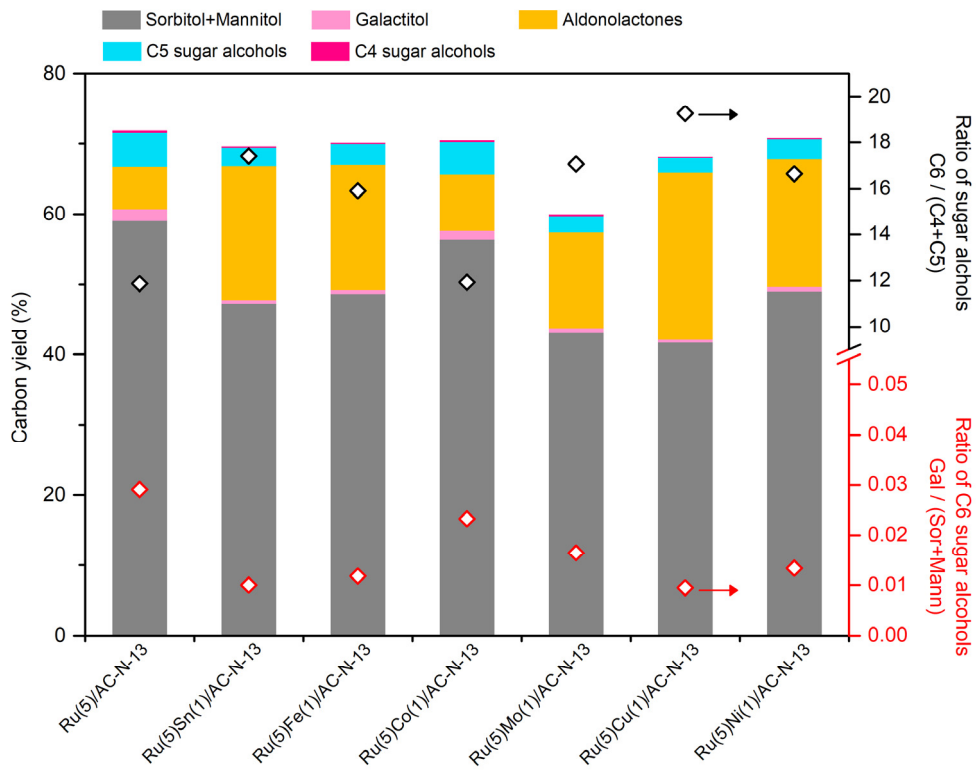

Figure 3-1. Product distribution over various bimetallic carbon catalysts at 150 °C for 3 h under 50 bar of H_2. C6 sugar alcohols: sorbitol (Sor), mannitol (Mann), and galactitol (Gal); C5 sugar alcohols: xylitol, arabitol, and ribitol; C4 sugar alcohols: threitol and erythritol; Aldonolactones: glucono-1,5-lactone and mannono-1,4-lactone.

3.3.2. Hydrogenation of alginic acid over RuCu bimetallic catalysts

To investigate the effect of Cu addition, catalysts were applied to the reaction after various amounts of Cu were loaded to 5 wt% Ru. Conversion of alginic acid over the catalysts was indirectly measured by GPC due to difficulty in separating unreacted alginic acid from the reaction mixture [30, 63]. As shown in GPC chromatograms (Figure 3-2), the reactant was fully converted to smaller molecules over bimetallic catalysts in all cases. However, a peak corresponding to a compound having molecular weight higher than a C6 sugar alcohol was observed. For comparison, a sugar alcohol with 12 carbon atoms, namely maltitol, was analyzed. The general trend of the increase in the intensity of such higher MW compound is in line with the increase in Cu content. It has been previously suggested that, under pressurized H_2 atmosphere, spilled-over hydrogens by a metallic site can result in the formation of protonic acid sites that could catalyze the hydrolysis of cellulose [44]. Similarly, the ability of Ru to catalyze the hydrolysis of C-C bonds in cellobiose into glucose has been also reported [13]. Thus, the above result implies that the addition of Cu could partly cover the active surface of Ru for hydrogen spillover, resulting in lowered hydrolysis activity and unconverted oligomeric compounds when the amount of Cu was increased. As summarized in Table 3-1, acid densities of catalysts measured by back titration under atmospheric condition exhibited an inverse correlation with the amount of Cu loaded. This might arise partly from the deposition of Cu on surface acidic oxygenates formed after oxidation of activated carbon with nitric acid. It has been previously reported that surface oxygenates of an oxidized carbon material could act as anchoring sites for a metal which eventually affects its dispersion [64].

As shown in Figure 3-3, Ru catalysts added with varied amounts of Cu exhibited different activities. The yield of target C6 sugar alcohols, sorbitol and mannitol, was greatly improved from 33.3% to 47.4% when 1 wt% of Cu was added. However, further increase of Cu content to 3 wt% and 5 wt% reduced yields of the target product to 15.2% and 5.0%, respectively. Surprisingly, the yield was partially recovered to 18.0% when the loading amount of Cu was increased to 10 wt%. In addition, it was found that pure Cu itself, Cu(10)/AC-N-13, was inactive in the hydrogenation of alginic acid. To investigate such unusual catalytic behavior with the addition of Cu, physicochemical properties of these catalysts were analyzed as follows.

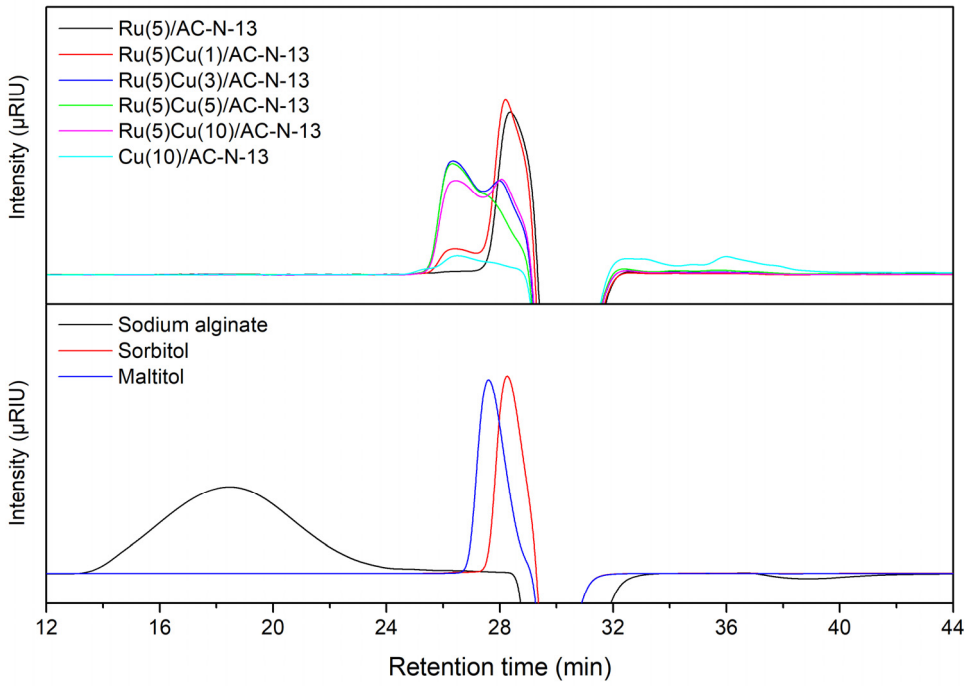

Figure 3-2. GPC chromatograms of liquid products obtained over monometallic and bimetallic catalysts at 180 °C for 2 h under 50 bar of H_2.

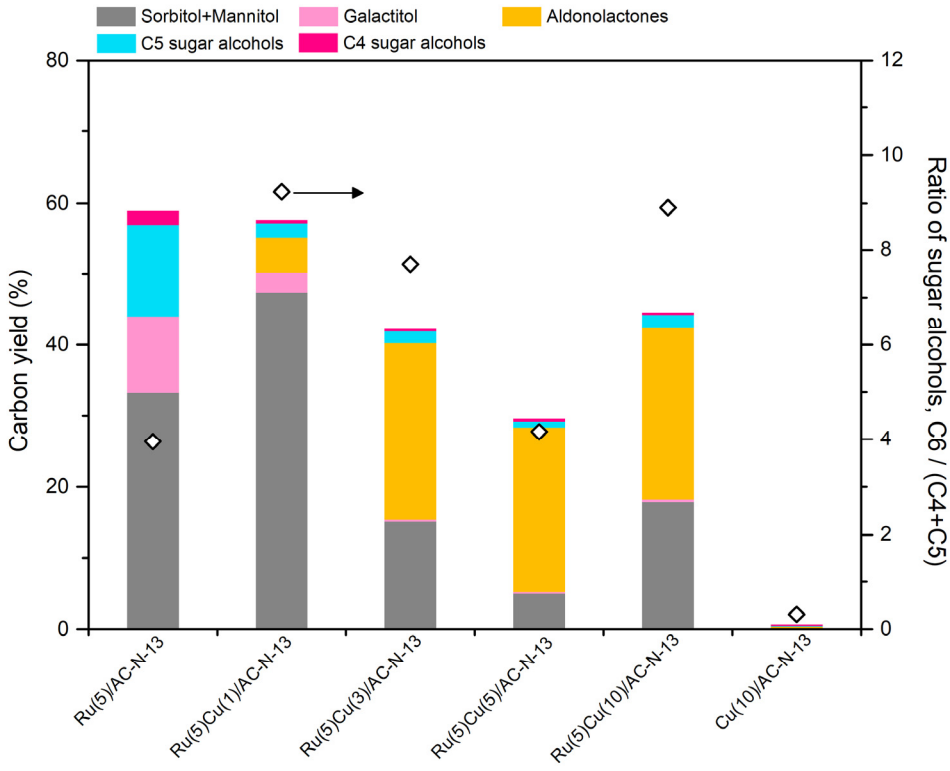

Figure 3-3. Product distribution over bimetallic and monometallic carbon catalysts at 180 °C for 2 h under 50 bar of H_2. C6 sugar alcohols: sorbitol, mannitol, and galactitol; C5 sugar alcohols: xylitol, arabitol, and ribitol; C4 sugar alcohols: threitol and erythritol; Aldonolactones: glucono-1,5-lactone and mannono-1,4-lactone.

Table 3-1. Textural properties of monometallic and bimetallic catalysts.

Catalyst	Specific surface area [a] (m^2/g catalyst)	Total pore volume [a] (cm^3/g catalyst)	Acid density [b] (mmol/g catalyst)
Ru(5)/AC-N-13	642.4	0.46	1.54
Ru(5)Cu(1)/AC-N-13	670.9	0.51	1.28
Ru(5)Cu(3)/AC-N-13	637.9	0.49	1.15
Ru(5)Cu(5)/AC-N-13	588.0	0.45	1.01
Ru(5)Cu(10)/AC-N-13	510.6	0.39	0.91
Cu(10)/AC-N-13	483.7	0.38	0.84

[a] Measured by N_2 adsorption-desorption.

[b] Measured by back titration.

3.3.3. Catalyst characterization

As shown in Figure 3-4, all ruthenium-based catalysts displayed type IV isotherm with H4 hysteresis, a representative of micro-mesoporous carbons [65]. As summarized in Table 3-1, when the amount of Cu was increased, surface area and pore volume of catalysts decreased from 642.4 to 510.6 m^2/g and from 0.46 to 0.39 cm^3/g, respectively, indicating partial pore blocking of the support.

As shown in Figure 3-5, in all samples, no diffraction pattern for Ru was detected, suggesting that Ru was well dispersed with average particle size below the detection limit of the instrument (<5 nm). On the other hand, diffraction peaks for Cu metal were observed for samples loaded with Cu at 5 wt% or higher. It was worth noting that Cu existed mainly in the metallic form in bimetallic catalysts in the bulk state while Cu_2O crystallite co-existed with metallic Cu in pure Cu catalyst. This suggests that the noble metal, Ru, can inhibit metallic Cu from being oxidized upon exposure to air during passivation [66].

Surface oxidation states of Ru and Cu on the activated carbon were investigated by XPS. As shown in Figure 3-6, a positive shift (ca. 0.4 eV) for Cu^0 (932.5 eV) in Cu 2p spectra was observed along with a negative shift (ca. 0.8 eV) for Ru^0 (462.8 eV) in Ru 3p spectra when the loading amount of Cu was increased compared to each monometallic catalyst. This result is inconsistent with previous studies concerning the direction of electron transfer between Ru and Cu. Previous XPS studies have proposed that an electron transfer from Ru to Cu can occur for silica supported RuCu bimetallic catalysts [67-68]. However, electron transfer from Cu to Ru has also been suggested based on infrared spectroscopy of CO adsorbed on RuCu supported on silica [69]. The result obtained in the present study indicates that

electron transfer is more likely to occur from Cu to Ru. Copper in its oxidation state of Cu^{2+} was also observed, which could be characterized by broad satellite peaks (939-946 eV and 960-965 eV) on the side of main peaks which partially screened by large Cu^0 peak [70]. Unfortunately, the oxidation state of Cu^+ could not be characterized since photoelectron peaks for Cu^+ overlapped with those of Cu^0. The effect of Cu addition was further investigated by chemisorption analysis as follows.

Results of H_2- and CO-chemisorption are summarized in Table 3-2. As indicated in the last row of Table 3-2, Cu was unable to chemisorb H_2 or CO under the condition studied [71]. This corresponds well to the inactive nature of Cu in hydrogenation of alginic acid as already shown in Figure 3-3. A general trend of decrease in the amount of CO adsorbed was observed with the addition of Cu with the exception of Ru(5)Cu(10)/AC-N-13. This result implies that the number of active Ru exposed is decreased due to partial coverage of Ru surface by Cu [58, 69]. The decrease in the yield of sorbitol and mannitol correlated well with the decrease in the active Ru sites measured by CO chemisorption. Similarly, with the exception of Ru(5)Cu(1)/ and Ru(5)Cu(10)/AC-N-13, the amount of hydrogen adsorbed exhibited a decreasing trend with increasing Cu content. The higher amount of hydrogen adsorption for Ru(5)Cu(1)/AC-N-13 than for Ru/AC-N-13 implies facile hydrogen spillover from Ru to Cu due to their intimate contact [58, 72-73]. Thus, Ru(5)Cu(1)/AC-N-13 could retain its ability of hydrogen activation and hydrogenation, although Ru surface was partially screened by Cu. Increases in amounts of hydrogen and CO adsorption were also observed for Ru(5)Cu(10)/AC-N-13. Such increases might indicate separation of Cu from Ru surface at high Cu loading [72, 74]. In this regard, restoration of the hydrogenation activity to some

extent for Ru(5)Cu(10)/AC-N-13 could be explained by the recovery of active Ru surface. Similar behavior was further evidenced by H_2-TPR as shown below.

Reducible behavior of each catalyst was then investigated by H_2-TPR. Results are shown in Figure 3-7. Monometallic Ru(5)/AC-N-13 exhibited one reduction peak at ca. 130 °C which could be assigned to the reduction of Ru species [75-76] while Cu(10)/AC-N-13 exhibited two reduction peaks: one at 192 °C and the other broader one at 261 °C that could be assigned to the reduction of Cu^{2+} to Cu^{+} and Cu^{+} to Cu^{0}, respectively [77]. Interestingly, reduction peak of Ru species shifted to higher temperature by 7 °C for bimetallic Ru(5)Cu(1)/AC-N-13 compared to monometallic Ru(5)/AC-N-13. This result might indicate the presence of a strong interaction between Ru and Cu, forming bimetallic clusters [69, 78]. When Cu loading amount was more than 1 wt%, the reduction peak of Ru species shifted back to ca. 130 °C and the reduction peak of CuO_x appeared. These above results further support the separation of Cu from Ru surface when Cu content was increased. Compared to monometallic Cu catalyst which exhibited two reduction peaks, the reduction peak of Cu^{+} shifted to lower temperature for all bimetallic catalysts except Ru(5)Cu(1)/AC-N-13, resulting in one broad reduction peak near 205 °C. This might indicate the intimate contact between Cu and Ru which could give rise to facile reduction of Cu oxides with the aid of Ru by means of hydrogen spillover, thus overlapping two CuO_x reduction peaks [79-80].

To further investigate the bimetallic interaction, XAS was conducted. Figure 3-8(b) shows k^2-weighted Fourier-transformed EXAFS spectra for these catalysts. For Ru(5)Cu(1)/ and Ru(5)Cu(3)/AC-N-13, a backscattering peak with interatomic distance of ca. 2.55 Å was observed. This could be attributed to multiple interatomic

interactions longer than Cu-O and Cu-Cu, implying RuCu bimetallic entities and a strong interaction between Cu and Ru as discussed in the H_2-TPR result [58, 81]. Although the above result was similar to previous researches, the extent of the interatomic interaction between Ru and Cu was relatively low compared to that in previous studies. There have been contradictory opinions regarding the presence of RuCu bimetallic entities. The controversy lies between a formation of bimetallic clusters as evidenced by EXAFS and a simple masking of active Ru surface as evidenced by H_2-chemisorption [74]. In addition, different extent for the formation of RuCu bimetallic clusters on various supports has been previously discussed. It has been suggested that a stronger metal-support interaction can result in a lower degree of the formation of RuCu bimetallic aggregates [82]. Thus, a lower degree of the formation of RuCu bimetallic clusters in the present study compared to previous researches might be due to a strong metal-support interaction induced by surface oxygenates of AC-N-13.

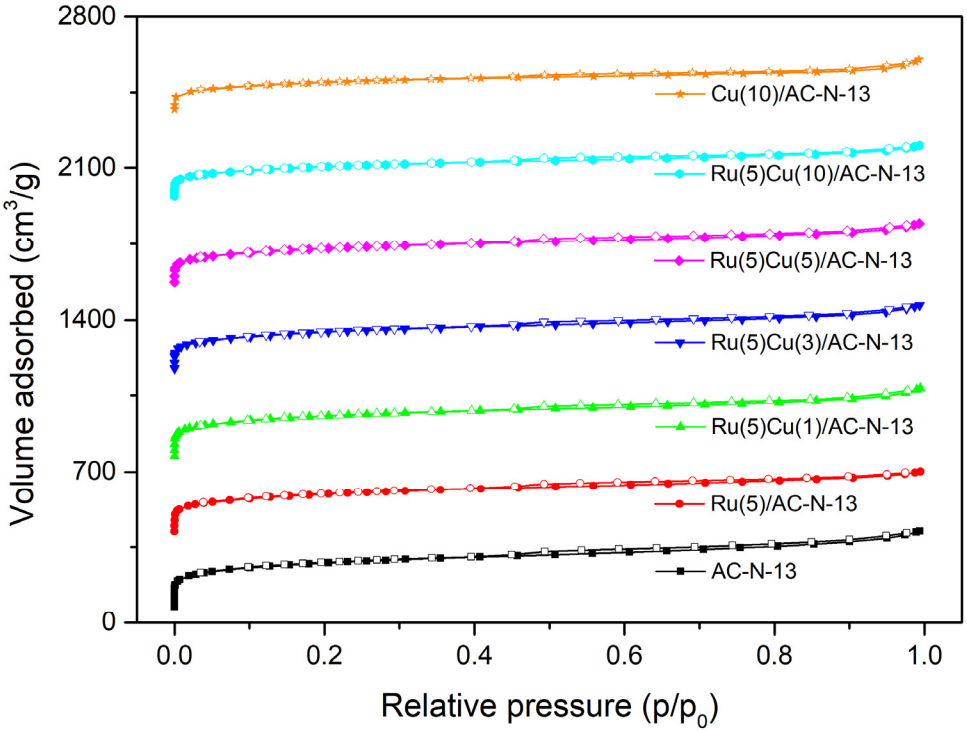

Figure 3-4. N_2 adsorption-desorption isotherms of monometallic and bimetallic catalysts.

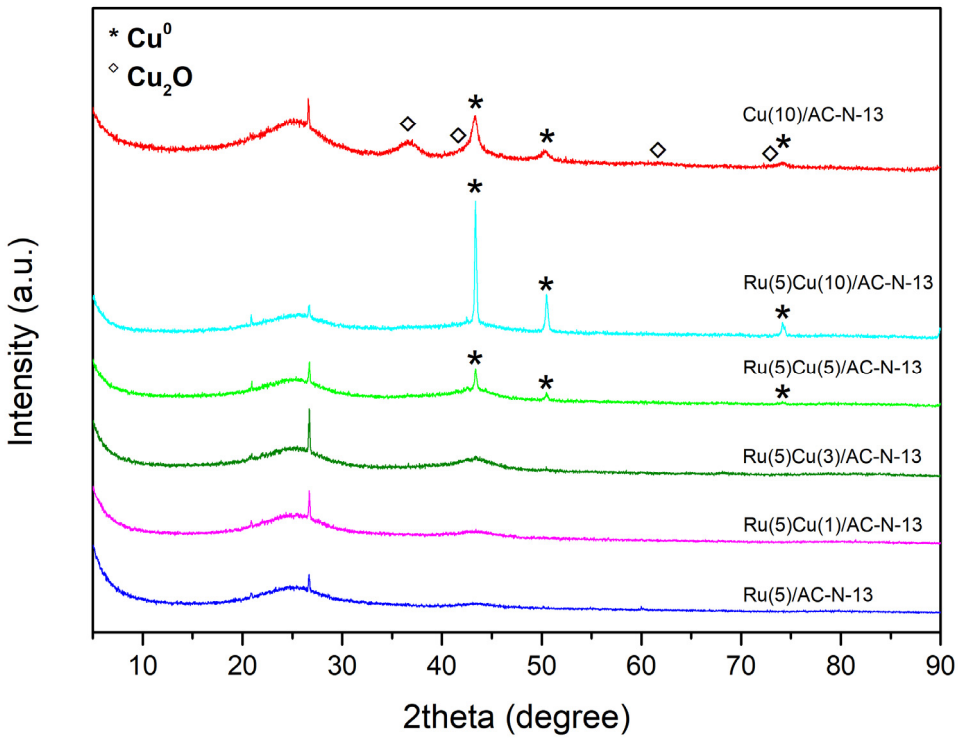

Figure 3-5. XRD diffractograms of monometallic and bimetallic catalysts.

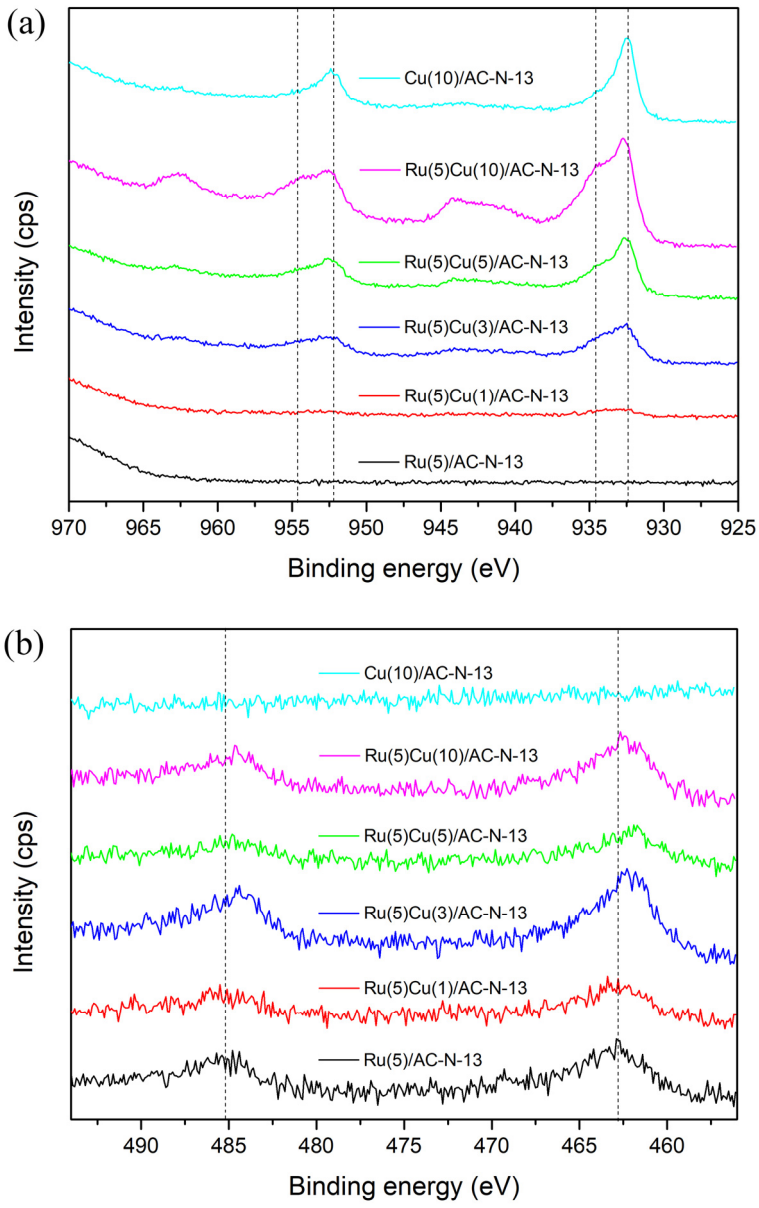

Figure 3-6. XPS spectra of (a) Cu 2p and (b) Ru 3p of bimetallic and monometallic catalysts.

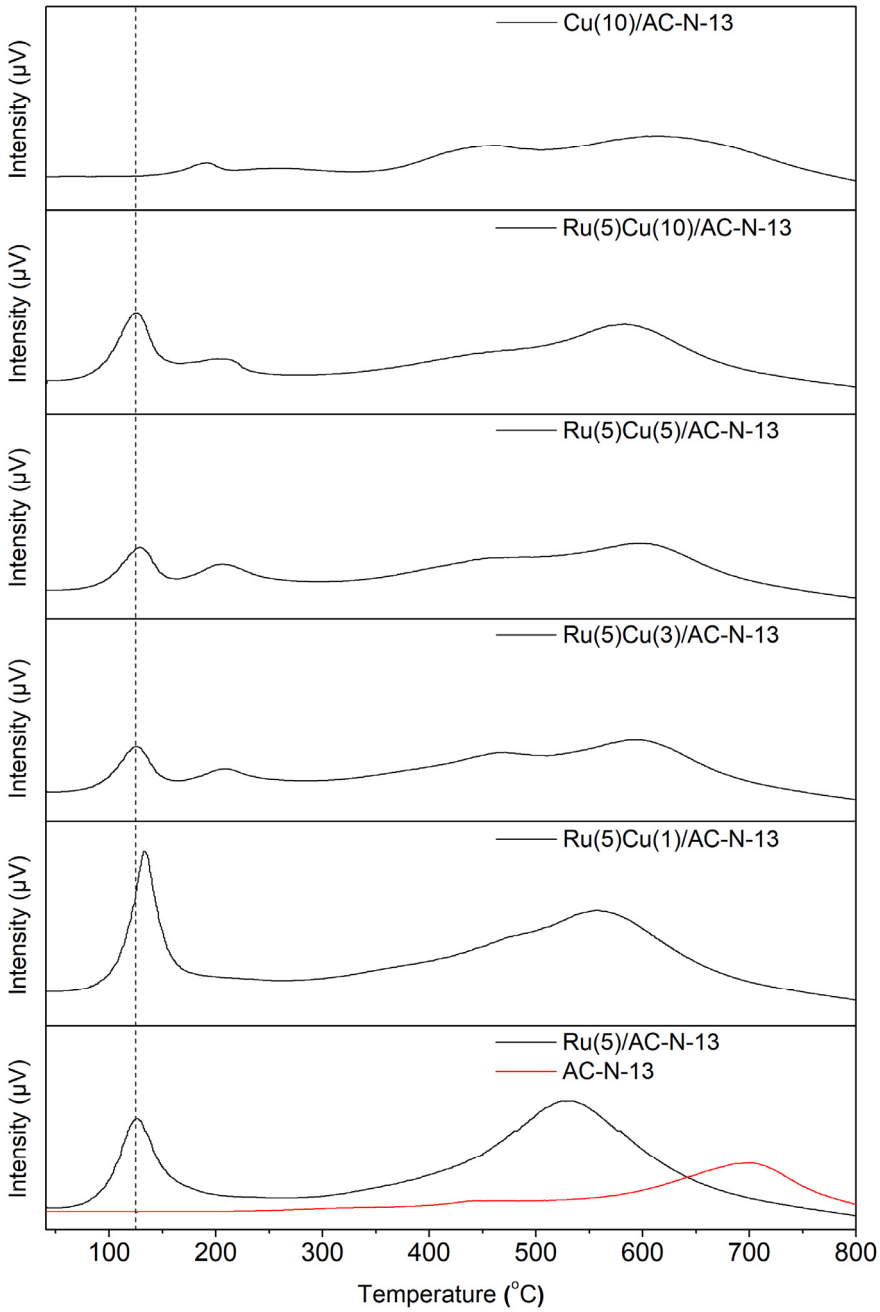

Figure 3-7. H_2-TPR profiles of the support, monometallic, and bimetallic catalysts.

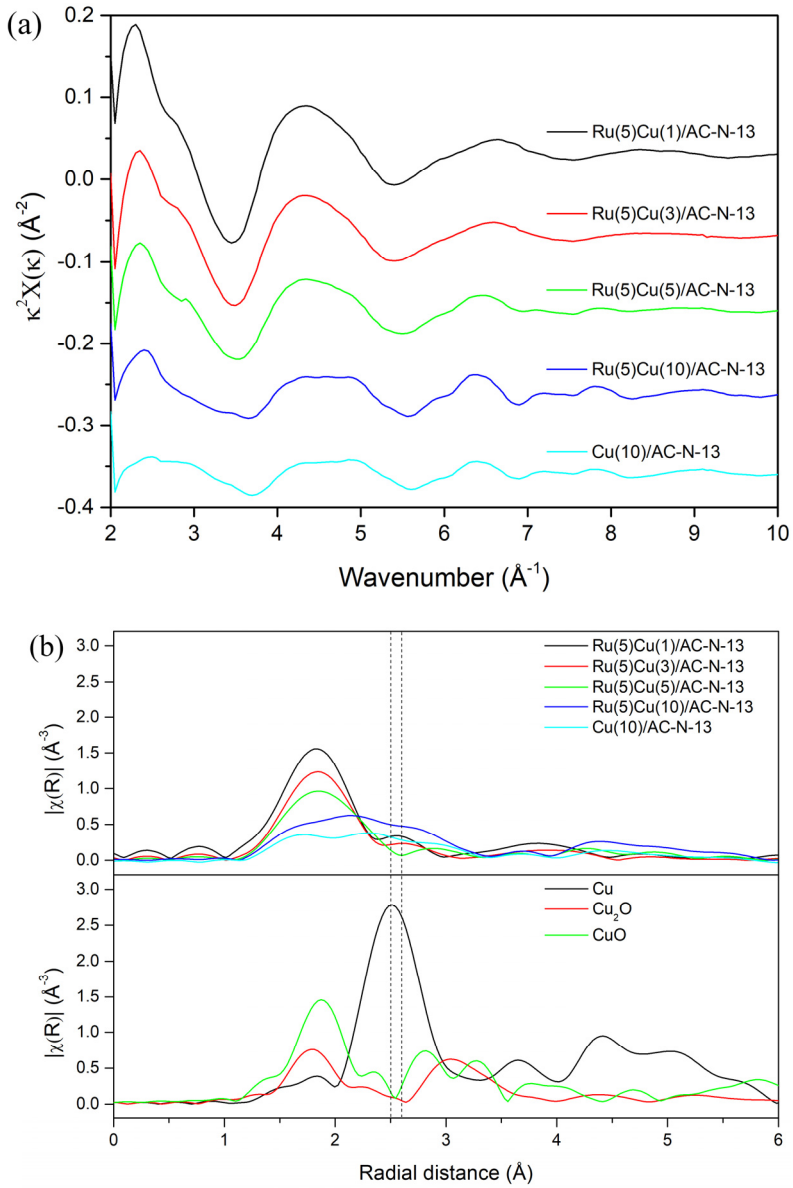

Figure 3-8. (a) k^2-weighted Cu K-edge EXAFS spectra for the catalysts and their (b) Fourier-transforms. The spectra were taken over the wavenumber range of $2.1 \leq K \leq 8.9$ Å^{-1}.

Table 3-2. H_2- and CO-Chemisorption results of monometallic and bimetallic catalysts.

Catalyst	Relative adsorbed amount of H_2/Ru [a]	Relative adsorbed amount of CO/Ru [a]
Ru(5)/AC-N-13	1.00	1.00
Ru(5)Cu(1) /AC-N-13	1.73	0.93
Ru(5)Cu(3) /AC-N-13	0.55	0.50
Ru(5)Cu(5) /AC-N-13	0.11	0.22
Ru(5)Cu(10) /AC-N-13	0.31	0.53
Cu(10) /AC-N-13	- [b]	0.01

[a] The values were normalized by the adsorbed amount of each adsorbate on Ru(5)/AC-N-13

[b] Slightly negative value was observed.

3.3.4. Stability of RuCu bimetallic catalyst

Long-term stability of a catalyst is crucial for practical application of catalysts. To investigate the durability of Cu-promoted Ru catalyst, the catalyst was subjected to repeated reactions. As shown in Figure 3-9, the catalyst was deactivated after each reaction. The decrease in the activity corresponded well to the amount of leached Cu. More than 80% of initial Cu was leached into the reaction mixture while the amount of leached Ru was less than 2%. The yield of target C6 sugar alcohols after the fourth reaction was 31.4% which was similar to that of unpromoted Ru(5)/AC-N-13 (33.3%). Thus, the deactivation arose from the leaching of Cu rather than from that of Ru, losing the synergistic effect caused by Cu addition. The above result led me to the next chapter to design a more stable Ru-based catalyst.

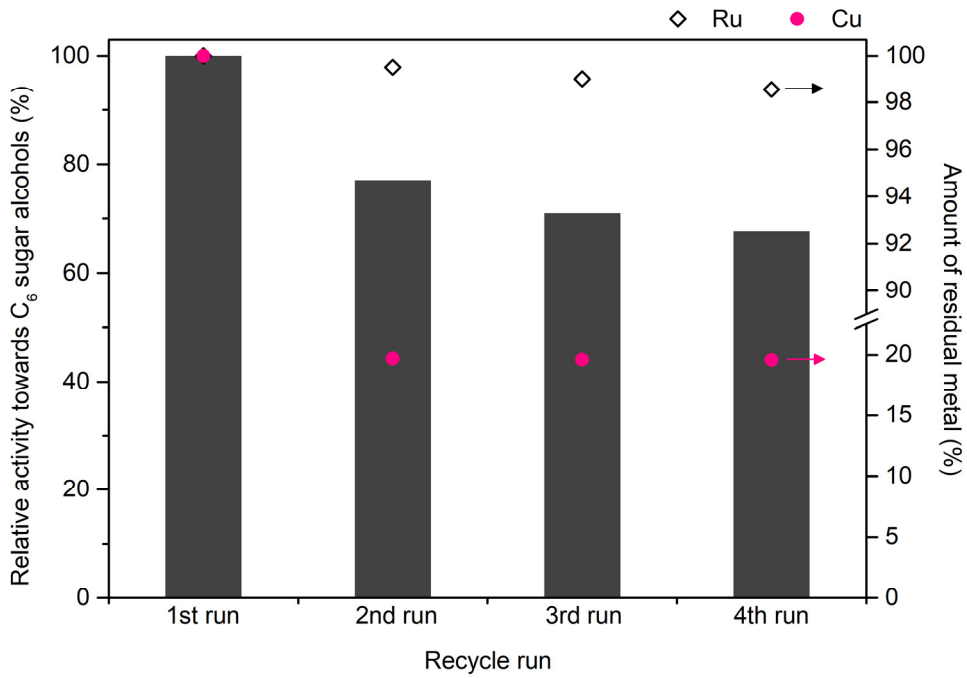

Figure 3-9. Recyclability test of Ru(5)Cu(1)/AC-N-13 at 180 °C for 2 h under 50 bar of H_2.

Chapter 4. Catalytic Hydrogenation of Alginic Acid into Sugar Alcohols over Ruthenium Supported on Nitrogen-doped Mesoporous Carbons

4.1. Introduction

As discussed in the preceding chapters, Ru-based carbon catalysts exhibited the deactivation owing to the leaching and/or aggregation of active metals. It is of great importance to improve the durability of catalysts for the practical application of heterogeneous catalysts.

The leaching or aggregation of an active metal could be prevented to certain degree by modifying a catalyst. To date, several methods, such as the addition of promoters, the control of pretreatment or synthesis condition, and deposition of thin layer on active metals with metal oxides or carbon, have been reported [83-84]. Aside from these strategies, introduction of nitrogen into carbon materials is also known to enhance the stability of catalysts. Defects created by N-doping could act as an anchoring site for metal species, thereby increasing the binding energy of metal nanoparticles to the carbon support [85-88]. The resultant catalysts displayed the strong metal-support interaction, thus having unique catalytic activity and stability. With their superior properties, N-doped carbon catalysts have found their application in various fields such as oxygen reduction reaction [89-91], hydrogen production via formic acid decomposition [92], and (transfer) hydrogenation [93-94] and oxidation reactions [95]. For instance, Pd and Ru nanoparticles stabilized by N-doped carbon

support have been used for dehydrogenation of formic acid and CO_2 hydrogenation, respectively [96-97]. Furthermore, it has been reported that even single atoms of Pt-group metals and Ni can be stabilized on N-doped carbons [98-99].

In this chapter, Ru supported on N-doped mesoporous carbon was synthesized and applied in the hydrogenation of alginic acid to produce sorbitol and mannitol for the first time. The effect of N-doping on the catalytic activity and on the stability of the catalyst was examined.

4.2. Experimental

4.2.1. Materials

Alginic acid was supplied from Sigma-Aldrich. Polyols (sorbitol, mannitol, galactitol, arabitol, ribitol, xylitol, glycerol, and propylene glycol), sugars (glucose and mannose), and glucono-1,5-lactone were obtained from Alfa Aesar. Mannono-1,4-lactone was purchased from TCI Chemicals. These above standard samples were used without further purification for 3-point calibration curves of GC. Urea, colloidal silica (Ludox HS-40), and sodium hydroxide were purchased from Sigma-Aldrich. Hydrochloric acid was supplied from Samchun Chemical Co., Ltd.

4.2.2. Catalyst preparation

N-doped mesoporous carbons were synthesized using previously reported methods with slight modifications as shown in Scheme 4-1 [100]. Briefly, glucose and urea with varied ratios (urea/glucose=0, 0.05, 0.1, 0.2, 0.4) were mixed with a proper amount of distilled water which contained HCl with glucose/HCl ratio of 10 (w/v). After a complete dissolution, an appropriate amount of Ludox HS-40 was poured into the above solution and magnetically stirred for ca. 5 h at 80 °C until it became a brownish gel. The mixture was then dried in an oven for 15 h at 160 °C followed by being crushed into powder. The resultant powder was carbonized in N_2 stream for 2 h at 300 °C and for 2 h at desired temperatures. Finally, silica spheres in the carbon material were then etched in 2 M of NaOH for 4 h at 85 °C to yield N-doped mesoporous carbon. Ruthenium of 5 wt% was impregnated onto the resultant

carbons using the conventional wet impregnation method. These catalysts were denoted as Ru(5)/NMC(x)(y) where x and y represented the ratio of urea/glucose and the carbonization temperature, respectively. Before being used in the hydrogenation reaction, Ru(5)/NMC(x)(y) was reduced at 300 °C for 3 h under 10% H_2 stream (100 ccm) followed by passivation under 5% O_2 stream (100 ccm) at room temperature for 0.5 h. Ruthenium chloride on a N-doped mesoporous carbon was fully reduced below 300 °C.

4.2.3. Catalyst characterization

X-ray diffraction (XRD) patterns were taken with an X-ray diffractometer (Rigaku). Voltage and current for X-ray generation with CuKα raditation were set at 40 kV and 30 mA, respectively. Elemental analysis (EA) was conducted with an elemental analyzer (Thermo Fischer). Back titration was conducted according to a previously reported method to measure the acid density of the catalysts using 0.01 M of NaOH and 0.02 M of HCl with few drops of phenolphthalein solution [30]. Inductively coupled plasma atomic emission spectroscopy (ICP-AES, PerkinElmer/Optima-4300 DV) was performed to measure the amount of ruthenium leached into the product solution after the reaction. N_2 adsorption-desorption technique was applied to measure BET (Brunauer-Emmett-Teller) surface area and BJH (Barrett-Joyner-Halenda) pore volume and BJH pore size distribution by using BELSORP-mini II (BEL JAPAN Inc.). Prior to the analysis, catalysts were degassed at 200 °C for at least 3 h. Dispersion and particle size of ruthenium were measured by CO chemisorption on BELCat (BEL JAPAN Inc.). Prior to CO pulse injection (4.98% CO/He, loop volume of 0.8570 cm^3), the catalysts were pretreated at 300 °C

for 2 h under 5% H_2 stream (50 ccm) and cooled down to 50 °C under He flow (50 ccm). X-ray photoelectron spectroscopy (XPS) was performed to investigate surface chemical states of ruthenium with an Al Kα μ-focused monochromatic source (1486.6 eV) in K-alpha (Thermo Scientific). The C 1s peaks of all catalysts were calibrated to 284.5 eV. Temperature programmed reduction (TPR) and desorption (TPD) were conducted on a BEL-CAT BASIC (BEL JAPAN Inc.) with a thermal conductivity detector (TCD). For H_2-TPR, a sample was pretreated at 150 °C for 2 h under Ar (50 ccm). After cooling down to 40 °C, the sample was heated to 900 °C (10 °C/min) under 5% H_2/Ar (50 ccm) and H_2 consumption was detected by TCD. For H_2-TPD, a sample was pre-reduced and H_2 was adsorbed at 300 °C for 2 h under 5% H_2/Ar (50 ccm). After cooling to 40 °C under Ar flow (50 ccm), the amount of desorbed H_2 was detected with TCD while the sample was heated to 900 °C (5 °C/min) under Ar flow (50 ccm).

4.2.4. Catalytic reaction

Catalytic hydrogenation of alginic acid was performed in a 100 mL stainless-steel autoclave (Parr Instrument Company). The vessel was charged with 0.1 g of 5 wt% Ru catalyst and 30 mL of distilled water containing 1% (w/v) of alginic acid. The reactor was purged with 50 bar of hydrogen three times to remove air. The autoclave was then pressurized with 50 bar of H_2 followed by heating to 180 °C. After 1 h, the reactor was quickly quenched in an ice-cold bath to prevent the further reaction. The autoclave was stirred with an impeller at a speed of 1000 rpm during the whole ramping and reaction time. The recyclability of the catalysts was tested via a multi-batch procedure as reported previously [30, 63].

4.2.5. Analytical method

The liquid product was analyzed by a gas chromatography (GC) equipped with a DB-5 (60 m × 0.25 mm × 0.25 μm) after being silylated using a method previously suggested to be able to lower high boiling points of sugar alcohols [59]. The carbon yield was determined as follows:

Carbon yield (%) = 100 × (number of carbon atoms in an organic compounds/6) × (moles of an organic compound in the product obtained by GC/moles of a repeating unit in alginic acid)

Gel permeation chromatography (GPC) was carried out by using Dionex Ultimate 3000 installed with a refractive index detector. Pullulan with a molecular weight range of 342-80500 was employed to calibrate the instrument. Total organic carbon (TOC) in the liquid product was analyzed by using a Sievers 5310 C (GE) equipped with an autosampler.

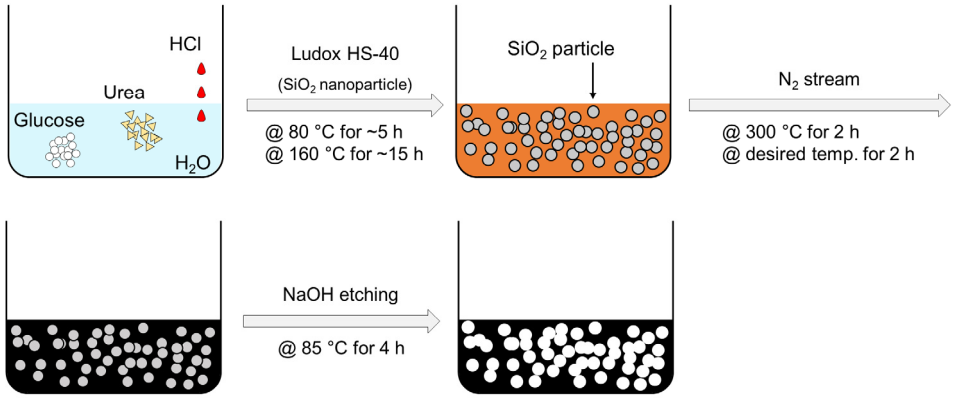

Scheme 4-1. A schematic synthesis procedure of nitrogen-doped-mesoporous carbon.

4.3. Results and discussion

4.3.1. Catalyst characterization

N-doped mesoporous carbons with varied nitrogen amounts were synthesized via a hard-templating method. The amount of nitrogen-doped was controlled by changing the amount of urea and carbonization temperature. To introduce a mesopore structure to the carbon materials, colloidal silica with an average particle size of 12 nm was used. These prepared Ru-based carbon catalysts exhibited similar acid density. Results are summarized in Table 4-1. As shown in Figure 4-1(a), when the ratio of urea/glucose was 0.1 and carbonization temperature was set to 700 °C, a uniform mesoporous structure was well developed with average pore diameter of ca. 8.2 nm, displaying a type IV isotherm and H2 hysteresis loop. Figure 4-1(b) displays the effect of carbonization temperature on the formation of mesoporous structure when the urea/glucose ratio was fixed at 0.1. All the carbon materials showed a distinctive mesoporosity with average pore size of 7.2-8.2 nm. As summarized in Table 4-2, all these carbons had high specific surface areas (> 980 m^2/g). Based on elemental analysis, the amount of nitrogen incorporated increased when the amount of urea increased and the carbonization temperature decreased. As shown in Figure 4-2 and Table 4-3, surface area and pore volume decreased due to the impregnation of ruthenium. CO chemisorption results showed that Ru nanoparticles were well dispersed on the support with an average particle sizes of around 4.5 nm. As displayed in Figure 4-3, all the carbon materials showed two broad X-ray diffraction patterns at around 24 ° and 44 ° assigned to amorphous carbon [101]. The same XRD patterns were observed after the nitrogen-doping and impregnation of Ru, indicating

that the amorphous structure of carbons was unaffected by the introduction of nitrogen or deposition of Ru. The absence of diffraction patterns of Ru species after the impregnation indicated that ruthenium was highly dispersed with average crystallite sizes below the detection limit of XRD which well corresponded to the values obtained by CO chemisorption.

XPS was conducted to investigate surface nitrogen species and electron states of Ru. As shown in Figure 4-4 and Table 4-4, four nitrogen species were identified after the introduction of nitrogen into mesoporous carbons, pyridinic-N (398.1 eV), pyrrolic-N (399.7 eV), quaternary-N (400.6 eV), and pyridinic-N-O (403.2 eV) [102]. The most notable feature was the increase in quaternary-N and pyridinic-N when the amount of urea increased. It is known that when carbonization temperature increased, the relative amount of quaternary-N increased due to its better thermal stability than the others [103]. Both quaternary-N and pyridinic-N could be involved in stabilizing metal particles according to a previous report [104]. It is understood that quaternary-N acting as an electron donator can delocalize and weaken π-π bonds of carbon atoms, resulting in the preferential adsorption of Pt atoms on carbon atoms activated by neighboring quaternary-N. In contrast, pyridinic-N can directly interact with the metal as an electron acceptor [105]. Electron-deficient Pt particles thus formed can interact more strongly with N-doped support via hybridization between d orbital of Pt and p orbital of pyridinic-N. In the present study, electron-deficient Ru species such as Ru^{3+} (464.6 eV) and Ru^{4+} (467.5 eV) were likely formed [106]. The relative amount of both Ru^{3+} and Ru^{4+} increased when the N/C atomic ratio increased. Specifically, the development of such oxidized Ru species corresponds better to the evolution of pyridinic-N than to that of quaternary-N. Therefore, it could be deduced

that pyridinic-N is more likely to interact with Ru nanoparticles in this study than quaternary-N.

Formation of RuO_x species could also be evidenced by H_2-TPR. Three reduction peaks were observed as shown in Figure 4-5. A broad peak in the range of 500-600 °C could be attributed to the methanation of carbon support catalyzed by ruthenium under hydrogen atmosphere [107]. The other two peaks could indicate the presence of reducible RuO_x species. The first peak at ca. 140 °C could be assigned to the reduction of Ru^{3+} to Ru^0 [108] while the second peak at ca. 230 °C could be ascribed to the reduction of Ru^{4+} to Ru^0 [109-110]. As summarized in Table 4-5, hydrogen consumption arising from the reduction of RuO_x increased as nitrogen content in mesoporous carbons increased. This result indicates that the incorporation of N favored the formation of RuO_x withdrawing electrons from Ru, which further confirms the certain interaction between dopant N and Ru.

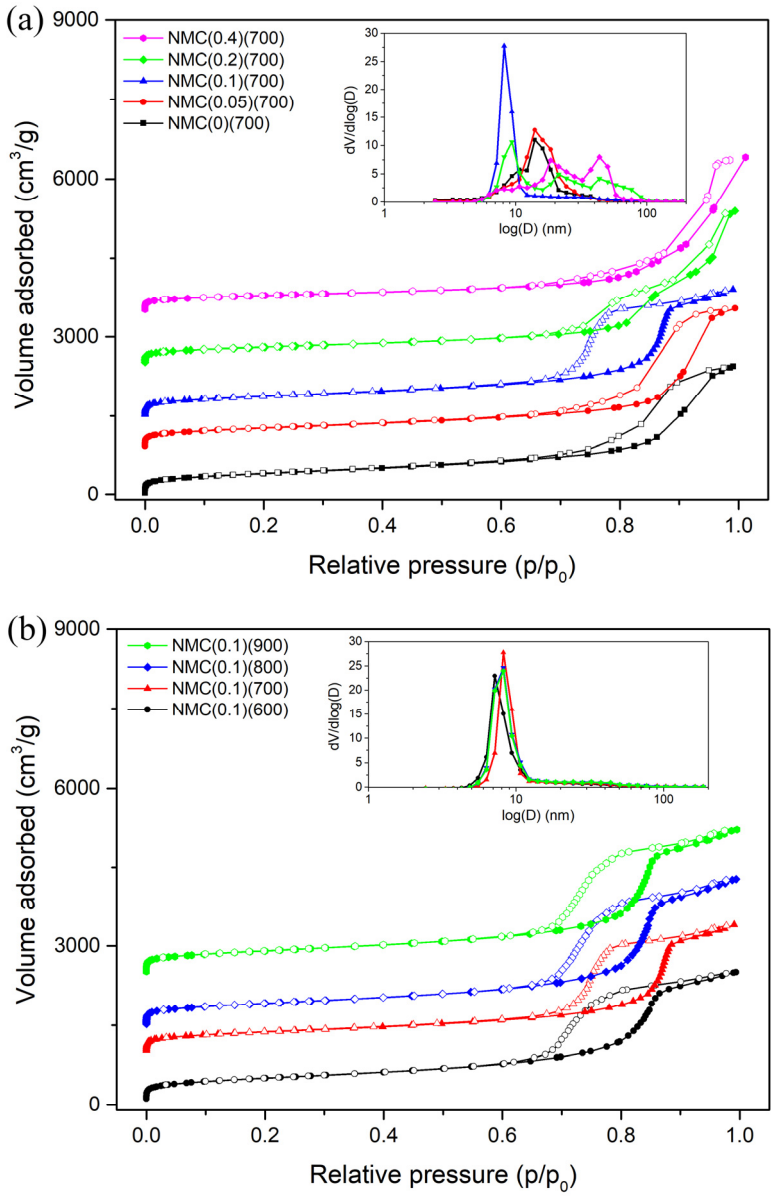

Figure 4-1. N_2 adsorption-desorption isotherms of (a) NMC(x)(700) and of (b) NMC(0.1)(y).

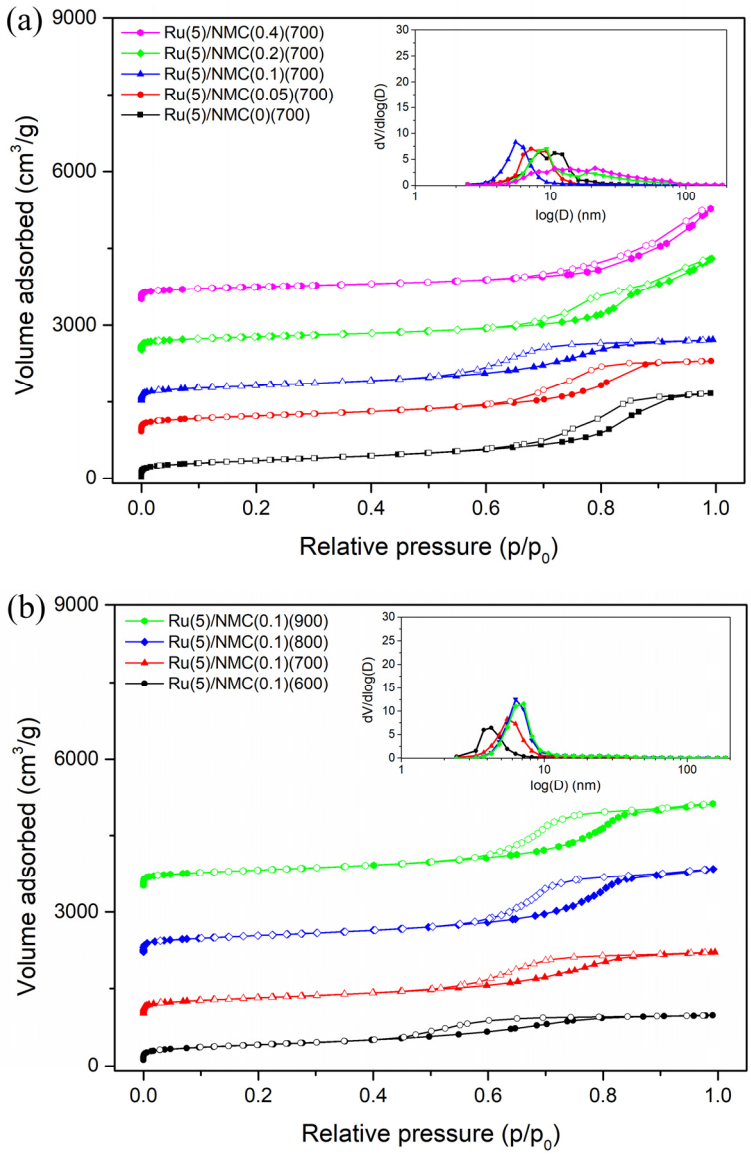

Figure 4-2. N_2 adsorption-desorption isotherms of (a) Ru(5)/NMC(x)(700) and of (b) Ru(5)/NMC(0.1)(y).

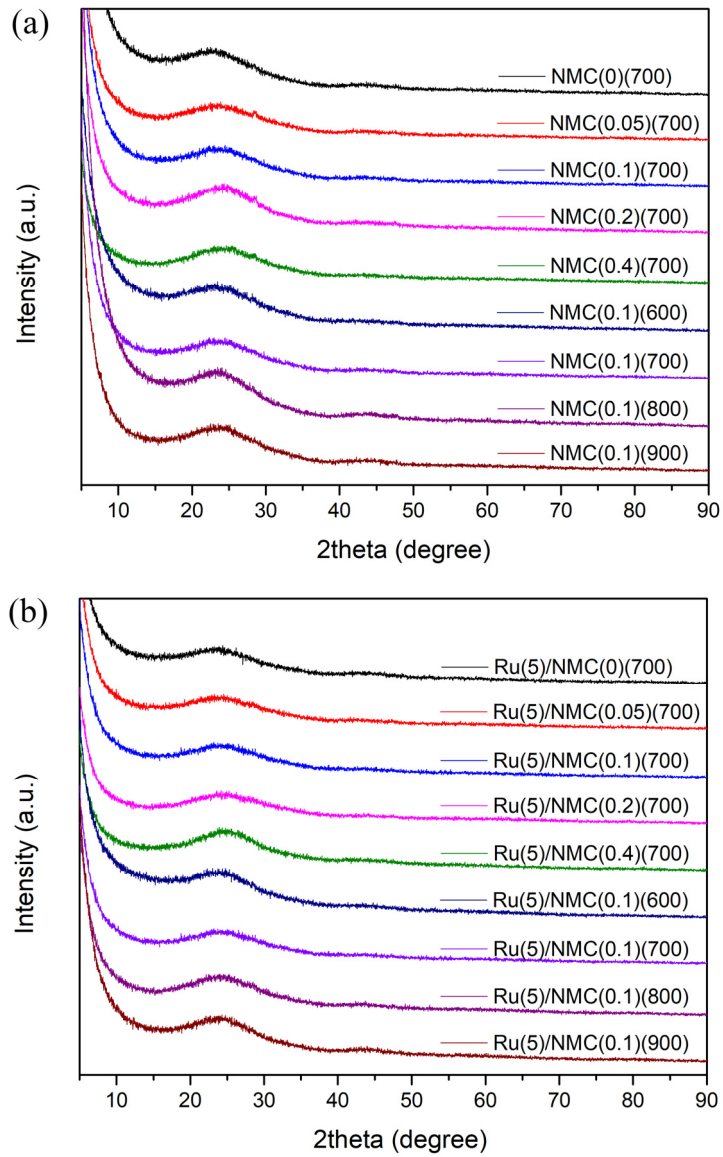

Figure 4-3. XRD diffractograms of (a) NMC(x)(y) and of (b) Ru supported on NMC(x)(y).

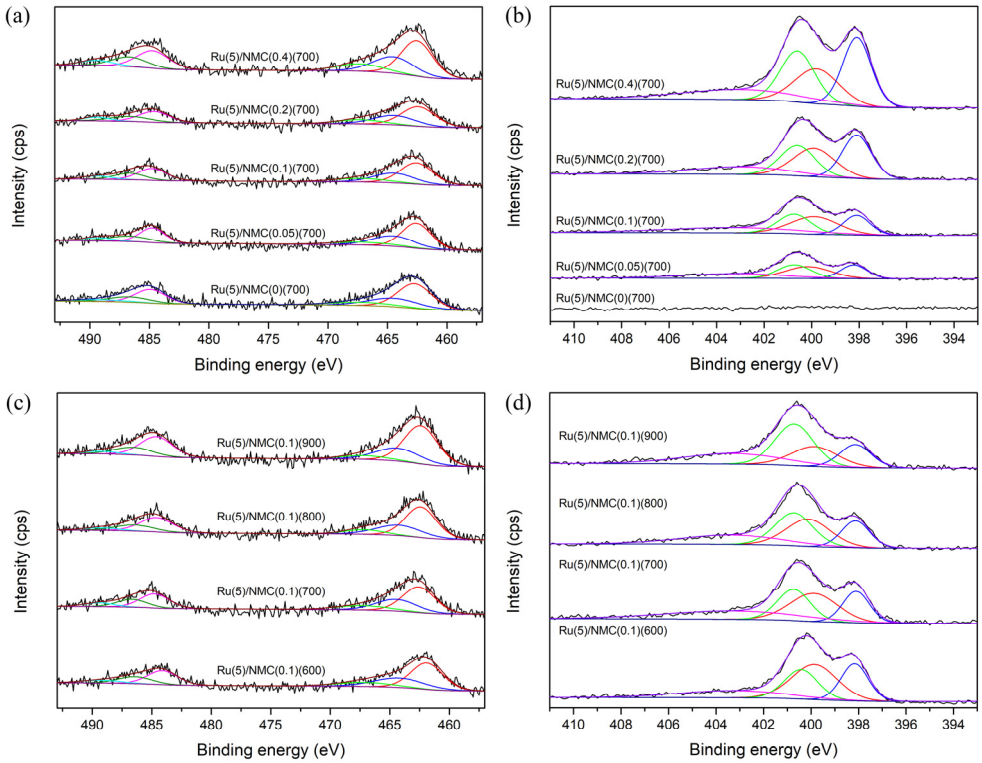

Figure 4-4. XPS spectra of (a) Ru 3p and (b) N 1s of Ru(5)/NMC(x)(700) and (c) Ru 3p and (d) N 1s of Ru(5)NMC(0.1)(y).

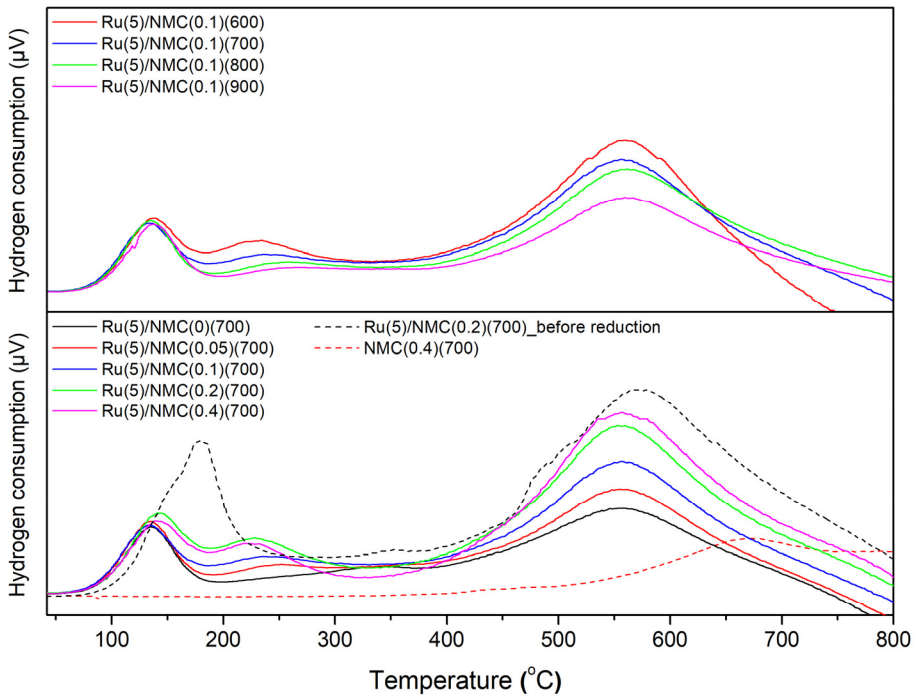

Figure 4-5. H_2-TPR profiles of Ru(5)/NMC(x)(y).

Table 4-1. Acid densities of Ru supported on N-doped mesoporous carbon catalysts.

Catalyst	Acid density [a] (mmol/g catalyst)	Catalyst	Acid density [a] (mmol/g catalyst)
Ru(5)/NMC(0)(700)	0.70	Ru(5)/NMC(0.1)(600)	0.85
Ru(5)/NMC(0.05)(700)	0.77	Ru(5)/NMC(0.1)(700)	0.84
Ru(5)/NMC(0.1)(700)	0.84	Ru(5)/NMC(0.1)(800)	0.81
Ru(5)/NMC(0.2)(700)	0.78	Ru(5)/NMC(0.1)(900)	0.76
Ru(5)/NMC(0.4)(700)	0.76		

[a] measured by back titration.

Table 4-2. Textural properties of N-doped mesoporous carbon catalysts.

Sample	Nitrogen [a] (%)	Surface area [b] (m^2/g)	Sample	Nitrogen [a] (%)	Surface area [b] (m^2/g)
NMC(0)(700)	0.0	1428.8	NMC(0.1)(600)	6.2	1447.5
NMC(0.05)(700)	2.0	1275.2	NMC(0.1)(700)	5.1	1302.8
NMC(0.1)(700)	5.1	1302.8	NMC(0.1)(800)	4.9	1457.4
NMC(0.2)(700)	9.9	1064.6	NMC(0.1)(900)	3.9	1435.9
NMC(0.4)(700)	11.4	982.6			

[a] measured by elemental analysis.

[b] calculated by BET method.

Table 4-3. Textural properties of Ru supported on N-doped mesoporous carbon catalysts.

Sample	Surface area [a] (m^2/g)	Crystallite size [b] (nm)	Dispersion [b] (%)
Ru(5)/NMC(0)(700)	1229.1	4.70	28.54
Ru(5)/NMC(0.05)(700)	1129.9	4.66	28.80
Ru(5)/NMC(0.1)(700)	1128.4	4.89	27.45
Ru(5)/NMC(0.2)(700)	958.9	4.48	39.98
Ru(5)/NMC(0.4)(700)	866.6	4.43	30.16

Sample	Surface area [a] (m^2/g)	Crystallite size [b] (nm)	Dispersion [b] (%)
Ru(5)/NMC(0.1)(600)	1122.4	4.48	29.81
Ru(5)/NMC(0.1)(700)	1128.4	4.89	27.45
Ru(5)/NMC(0.1)(800)	1215.8	4.18	32.14
Ru(5)/NMC(0.1)(900)	1148.8	3.71	36.18

[a] measured by elemental analysis.

[b] calculated by BET method.

Table 4-4. XPS deconvolution results of Ru(5)/NMC(x)(y).

Catalyst	Relative surface atomic percent (%)			Relative surface atomic ratio
	Ru^0	Ru^{3+}	Ru^{4+}	N/C (x 10^2)
Ru(5)/NMC(0)(700)	58.1	29.7	12.3	0.24
Ru(5)/NMC(0.05)(700)	54.5	32.0	13.5	2.75
Ru(5)/NMC(0.1)(700)	54.0	31.1	14.9	4.34
Ru(5)/NMC(0.2)(700)	53.0	31.7	15.4	6.40
Ru(5)/NMC(0.4)(700)	52.7	31.7	15.6	9.54
Ru(5)/NMC(0.1)(600)	54.6	30.5	14.9	6.28
Ru(5)/NMC(0.1)(800)	59.0	29.7	11.3	5.26
Ru(5)/NMC(0.1)(900)	62.7	28.5	8.8	4.25

Catalyst	Relative surface atomic percent (%)			
	Pyridinic-N	Pyrrolic-N	Quaternary-N	Pyridinic-N-O
Ru(5)/NMC(0)(700)	0	0	0	0
Ru(5)/NMC(0.05)(700)	20.0	29.6	25.1	25.3
Ru(5)/NMC(0.1)(700)	19.2	30.8	23.6	26.4
Ru(5)/NMC(0.2)(700)	29.8	27.9	24.8	17.5
Ru(5)/NMC(0.4)(700)	30.4	23.9	27.1	18.6
Ru(5)/NMC(0.1)(600)	23.3	36.7	22.7	17.4
Ru(5)/NMC(0.1)(800)	18.3	29.0	29.8	22.8
Ru(5)/NMC(0.1)(900)	16.9	21.3	37.0	24.8

Table 4-5. Consumption amounts of hydrogen measured by H_2-TPR of Ru(5)/NMC(x)(y).

Catalyst	Hydrogen consumption (μmol/g catalyst)	
	1st peak	2nd peak
Ru(5)/NMC(0)(700)	0.49	0.07
Ru(5)/NMC(0.05)(700)	0.52	0.12
Ru(5)/NMC(0.1)(700)	0.50	0.31
Ru(5)/NMC(0.2)(700)	0.61	0.58
Ru(5)/NMC(0.4)(700)	0.60	0.55

Catalyst	Hydrogen consumption (μmol/g catalyst)	
	1st peak	2nd peak
Ru(5)/NMC(0.1)(600)	0.55	0.56
Ru(5)/NMC(0.1)(700)	0.50	0.31
Ru(5)/NMC(0.1)(800)	0.53	0.21
Ru(5)/NMC(0.1) (900)	0.51	0.18

4.3.2. Effect of N-doping on catalytic hydrogenation of alginic acid

To produce sugar alcohols, batch-wise reactions were conducted over the above characterized catalysts (Figure 4-6). Degrees of depolymerization of alginic acid over different catalysts were measured indirectly by means of GPC since the unconverted alginic acid could not be easily separated from the product mixture [30, 63]. As displayed in Figure 4-7, the reactant was fully converted over all catalysts. In addition, TOC analysis results shown in Table 4-6 revealed that most of carbons were retained in the liquid phase, suggesting that carbon loss into gas phase was negligible. Thus, losses in the carbon balance could be attributed to the unidentified byproducts. As shown in Figure 4-6, hydrolytic hydrogenation of alginic acid mainly produced C6 sugar alcohols, sorbitol and mannitol. Unlike the case of cellulose hydrogenation, the catalytic reaction of alginic acid resulted in the concurrent production of both sorbitol and mannitol since alginic acid consists of two epimeric monomers [63]. The highest yield of target alcohols was obtained as 50.3% (sorbitol: 24.3% and mannitol: 26.0%) when Ru(5)/NMC(0.1)(600) was employed at 180 °C for 1 h. In addition to sorbitol and mannitol derived from these two monomers, the production of another C6 sugar alcohol, namely galactitol, was also observed. It has been reported that galactitol could be formed via epimerization of produced sugar alcohols during the hydrogenation of cellulose or glucose, resulting in the lower selectivity of the desired sugar alcohols [54]. A general trend of decrease in galactitol formation was observed as the amount of N-doped increased. Previous researches have suggested that epimerization of polyols could be catalyzed by metal sites in the presence of H_2 [53-54]. As already discussed above, since all the catalysts possessed nearly identical acid densities and average particle sizes of Ru, different activities

might arise from the doped nitrogen or from the modified electronic state of Ru species induced thereby. As already evidenced by H_2-TPR and XPS, ruthenium deposited on N-doped carbons was featured by a deficit of electron density. Thus, it could be deduced that RuO_x species on nitrogen-doped carbon are responsible for the suppression of the epimerization.

Another effect derived from N-doping is the inhibition of the production of lower sugar alcohols. The formation of C4 and C5 sugar alcohols from sorbitol follows terminal C-C cleavage by decarbonylation or internal C-C cleavage by retro-aldol reaction [111]. The proposed mechanism of the C-C scission involves a metallic site for dehydrogenation of sorbitol and hydrogenation of keto-intermediates [112-113]. Since the incorporation of N favors the formation of RuO_x, it could be assumed that oxidized Ru species are again responsible for the inhibition of further hydrogenolysis of sorbitol and mannitol to lower polyols.

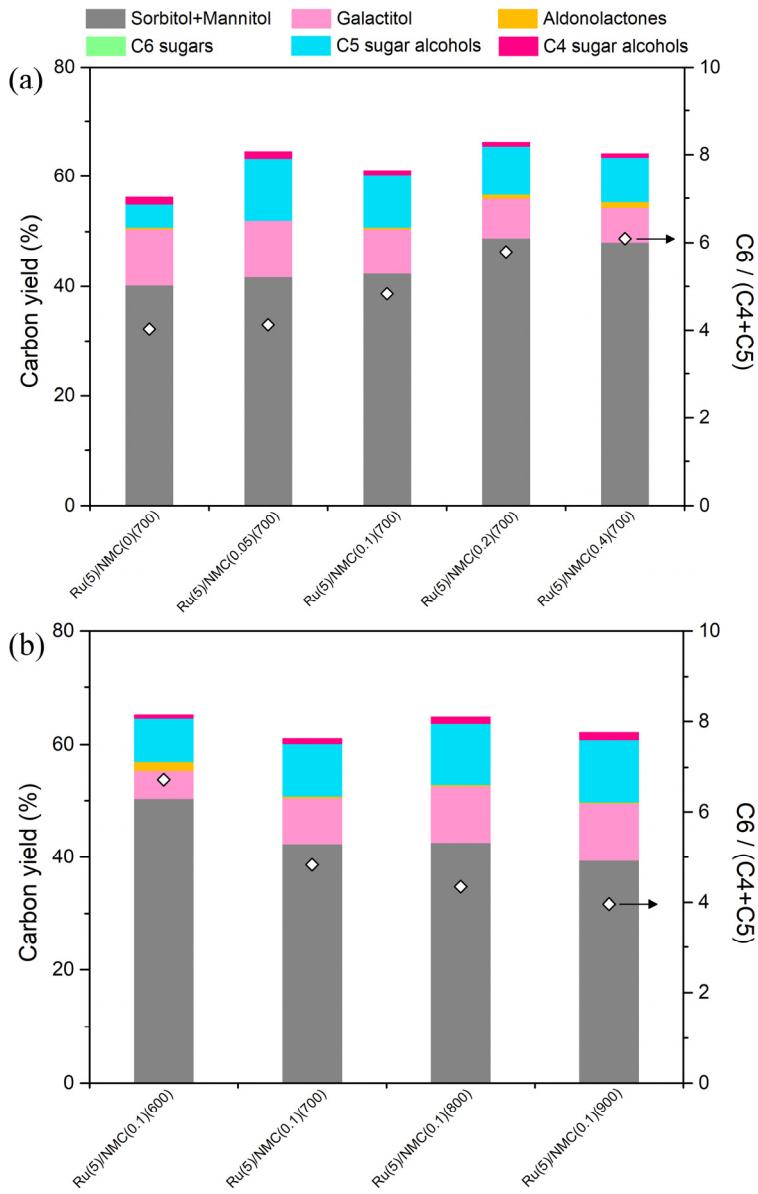

Figure 4-6. Product distribution over Ru supported on different N-doped mesoporous carbon catalysts at 180 °C for 1 h under 50 bar of H_2. Aldonolactones: glucono-1,5-lactone and mannono-1,4-lactone; C6 sugars: glucose and mannose; C5 sugar alcohols: xylitol, arabitol, and ribitol; C4 sugar alcohols: threitol and erythritol.

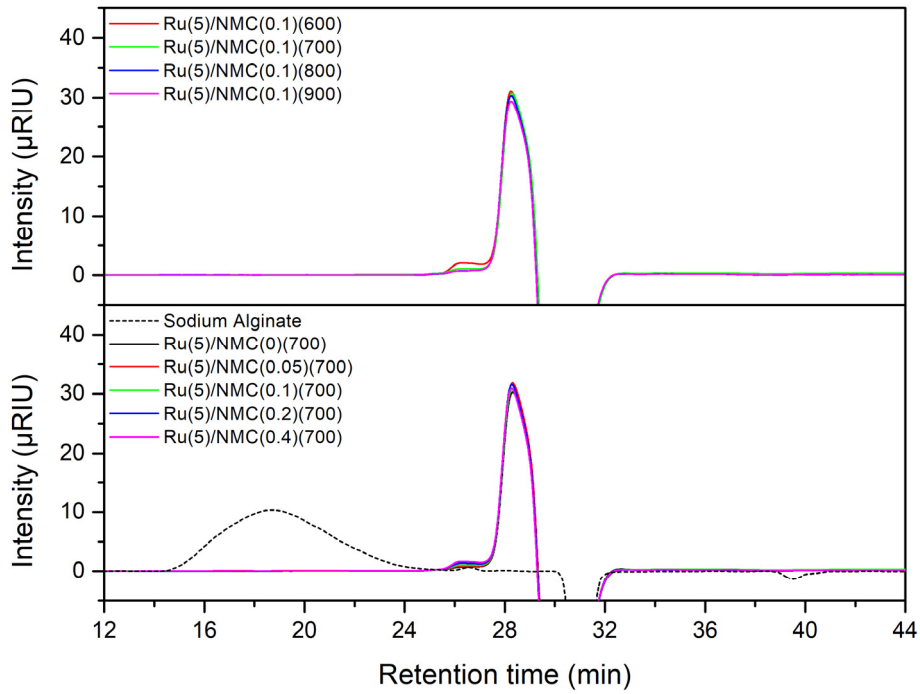

Figure 4-7. GPC chromatograms obtained after the reaction at 180 °C for 1 h under 50 bar of H_2.

Table 4-6. Total organic carbon in liquid products obtained after the reaction at 180 °C for 1 h under 50 bar of H_2.

Catalyst	TOC in liquid product [a] [mg/L]	TOC in liquid product [a] [%]
Ru(5)/NMC(0)(700)	16.3	94.4
Ru(5)/NMC(0.05)(700)	16.3	94.4
Ru(5)/NMC(0.1)(700)	16.6	96.1
Ru(5)/NMC(0.2)(700)	16.7	96.7
Ru(5)/NMC(0.4)(700)	16.8	97.3

Catalyst	TOC in liquid product [a] [mg/L]	TOC in liquid product [a] [%]
Ru(5)/NMC(0.1)(600)	16.5	95.6
Ru(5)/NMC(0.1)(700)	16.6	96.1
Ru(5)/NMC(0.1)(800)	16.2	93.8
Ru(5)/NMC(0.1)(900)	15.9	92.1

[a] values were calculated based on TOC of 1% alginic acid (17.3 mg/L)

4.3.3. Stability of the Ru supported on N-doped mesoporous carbon catalyst

Durability of a heterogeneous catalyst is a critical factor for a practical application. As already discussed in previous chapters, it was previously revealed that leaching and sintering of ruthenium were the main reasons for the deactivation of commercial Ru/C catalyst during the hydrogenation of alginic acid [63]. Furthermore, the deactivation was accelerated by the acidic nature of alginic acid, promoting the formation of a metal-carboxylate complex [47, 63, 114]. As shown in Figure 4-8, when ruthenium supported on N-doped carbon was subjected to repeated reactions, no appreciable deactivation was observed and the leaching of Ru was less than 1% as measured by ICP-AES. In addition, aggregation of the active metal was also negligible as evidenced by CO chemisorption (Table 4-7). Furthermore, no discernible decrease in specific surface areas or pore volumes even after the fourth reaction was observed, indicating no formation of coke. The strong interaction exerted between Ru and nitrogen-doped might have suppressed the formation of soluble $Ru(OH)_x$ species known to be responsible for the leaching of Ru [115].

The interaction between transition metal and nitrogen-doped could be explained by the hybridization of d orbital of transition metal with π orbital of nitrogen, which results in an intimate contact between metal and support [88, 116]. Previous researches have reported the beneficial effects of an intimate interfacial contact between ruthenium and carbon support on catalytic hydrogenation reactions [117]. Similarly, Arai et al. have reported the effect of interaction between Ru and supports on the adsorption strength of hydrogen [118]. They found that hydrogen adsorption was enhanced by the electron deficient ruthenium formed by electronegative supports. Experimentally, the intimate contact between metal and carbon support can

be evidenced by H_2-TPD [119]. As shown in Figure 4-9, H_2-TPD results displayed two hydrogen desorption peaks. The first peak at around 120 °C could be assigned to the desorption from hydrogen chemisorbed on metal surface, whereas the second peak at higher temperature, 300-400 °C, could be assigned to that from hydrogen chemisorbed on metal/support interface spilled-over from Ru to support [120]. The shift towards a lower desorption temperature of the second peak indicated that a stronger interaction was present when the nitrogen content increased. In addition, an increase in the desorption amount of hydrogen from metal/support interface was observed (Table 4-8). This confirms the facile hydrogen spillover from Ru to the support due to the strong interaction between Ru and N-doped carbon support.

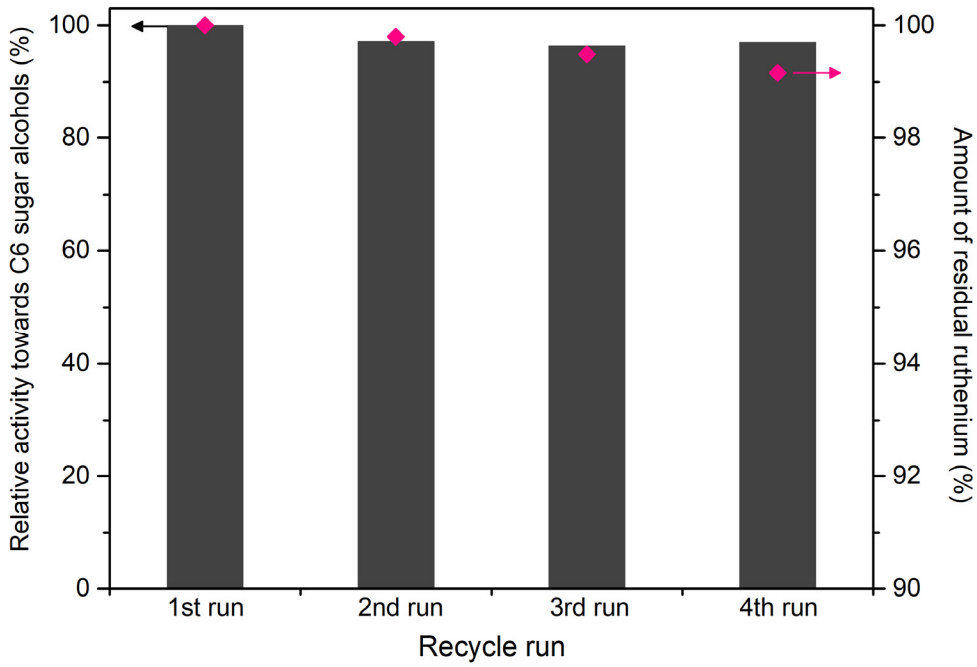

Figure 4-8. Recycle experiment conducted over Ru(5)/NMC(0.2)(700) at 180 °C for 1 h under 50 bar of H_2.

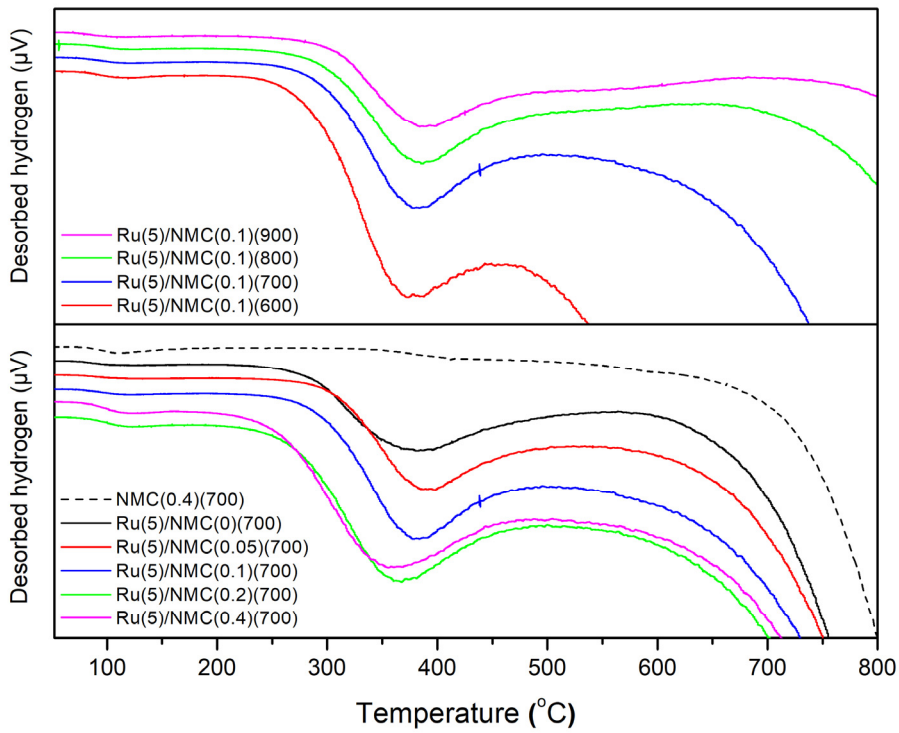

Figure 4-9. H_2-TPD profiles of Ru(5)/NMC(x)(y).

Table 4-7. Textural properties, particle sizes, and dispersions of spent catalysts.

Sample	Recycle run	Surface area [a] (m^2/g)	Crystallite size [b] (nm)	Dispersion [b] (%)
Ru(5)/NMC(0.2)(700)	1st (Fresh)	958.9	4.48	39.98
	2nd	909.1	4.15	32.37
	3rd	905.1	4.30	31.24
	4th	1039.9	5.15	26.03

[a] calculated by BET method.

[b] measured by CO chemisorption.

Table 4-8. Desorption amounts of hydrogen measured by H_2-TPD of Ru(5)/NMC(x)(y).

Catalyst	Hydrogen desorption (mmol/g catalyst)	
	1st peak	2nd peak
Ru(5)/NMC(0)(700)	0.005	0.260
Ru(5)/NMC(0.05)(700)	0.005	0.287
Ru(5)/NMC(0.1)(700)	0.007	0.309
Ru(5)/NMC(0.2)(700)	0.008	0.387
Ru(5)/NMC(0.4)(700)	0.010	0.440

Catalyst	Hydrogen desorption (mmol/g catalyst)	
	1st peak	2nd peak
Ru(5)/NMC(0.1)(600)	0.007	0.304
Ru(5)/NMC(0.1)(700)	0.007	0.309
Ru(5)/NMC(0.1)(800)	0.006	0.237
Ru(5)/NMC(0.1) (900)	0.006	0.235

Chapter 5. Conclusion and summary

Various ruthenium-based carbon catalysts were synthesized and applied to the catalytic hydrogenation of alginic acid for the selective production of sugar alcohols, mainly sorbitol and mannitol, for the first time.

Firstly, noble metals (Ru, Pd, Pt, Rh, and Ir) supported on carbon were used for the hydrogenation reaction. The highest yield of C6 sugar alcohols was obtained as 61% (sorbitol: 29%, mannitol: 28%, and galactitol: 4%) at 150 °C for 12 h under 50 bar of H_2 over ruthenium supported on carbon. Hexitols were mainly produced over Ru supported on carbon catalysts, whereas byproducts such as dideoxy-aldonic acids and their lactones were produced over Pd, Pt, Rh, and Ir supported on carbon catalysts. Based on the result of mass spectrometry analysis, the plausible reaction pathway of the hydrogenation of alginic acid was proposed. It was understood that alginic acid was depolymerized into chunks of oligomers in a random fashion. The hydrogenation of two reducible functional groups, carboxylic- and aldehyde-end, in dimeric intermediates led to the formation of 5 different partially hydrogenated intermediates which were then cleaved into C6 sugar alcohols over carbon-supported Ru. Unlike the cellulose hydrogenation, mannitol was produced as much as sorbitol due to the composition of alginic acid which is composed of two epimeric monomers and to the isomerization between produced hexitols. The leaching and aggregation of the active metal, Ru, after the reaction caused the deactivation of the catalyst.

Secondly, the effect of Cu addition to Ru supported on nitric acid-treated activated carbon catalyst on the hydrogenation of alginic acid was investigated. Both geometric and electronic effects were observed by H_2-TPR, H_2- or CO-

chemisorption, and XPS when Cu was added to Ru. The addition of Cu resulted in the blocking of active Ru surface and electron transfer between Ru and Cu. Furthermore, the addition of a proper amount of Cu, namely 1 wt%, resulted in the formation of RuCu bimetallic aggregates and a strong interaction between Ru and Cu as evidenced by H_2-TPR and XAS. Such intimate interaction between Ru and Cu gave rise to the facile hydrogen spillover from Ru to Cu, which enabled Ru to maintain its hydrogenation activity in spite of the decrease in active Ru surface exposed. The highest yield of target sugar alcohols was 47.4% (sorbitol: 26.9% and mannitol: 20.5%) when alginic acid was hydrogenated at 180 °C for 2 h over Ru(5)Cu(1)/AC-N-13, where numbers in parenthesis refer to loading amount (wt%) of each metal. Such RuCu bimetallic catalyst was deactivated over repeated reactions owing to leaching of Cu.

Lastly, to enhance the stability of the Ru-based carbon catalyst, Ru supported on nitrogen-doped mesoporous carbons were synthesized and applied to the hydrogenation of alginic acid. Introduction of nitrogen induced the interaction of Ru with the N-doped support, especially with pyridinic-N resulting in the formation of RuO_x species. In addition, the intimate interaction between ruthenium and N-doped support facilitated hydrogen spillover from Ru to the support. The oxidized Ru was found to suppress the side reactions such as epimerization and C-C cleavage. The highest yield of target C6 sugar alcohols was 50.3% (sorbitol: 24.3% and mannitol: 26.0%) when alginic acid was hydrogenated at 180 °C for 1 h under 50 bar of H_2 over Ru(5)/NMC(0.1)(600), where 0.1 and 600 refer to the urea/glucose ratio and carbonization temperature (°C), respectively. The catalyst exhibited the excellent hydrothermal stability under the reaction condition studied. The strong interaction

was proposed to be the origin of the inhibition of leaching and aggregation of Ru.

This first attempt to utilize alginic acid as a proper surrogate for cellulose to produce sugar alcohols would draw a worldwide attention into the field of a catalytic utilization of algal biomass and would alleviate the heavy dependence on lignocellulosic biomass for the production of renewable chemicals.

국 문 초 록

바이오매스는 탄소, 수소, 산소의 기본 원소를 포함한 유기화합물을 직접적으로 생산할 수 있는 신재생 원료로서, 석유 기반 연료 및 화합물의 대체를 위해 바이오매스 전환 기술 개발이 요구되고 있다. 해조류 바이오매스는 기존의 바이오매스(농작물 및 목질계 바이오매스)와는 달리, 비식용성이기 때문에 식량 문제와 상충되지 않고 생장 속도가 빠르다는 장점이 있다. 또한 난분해성 성분인 리그닌이 없기 때문에 그 분해 및 활용이 용이하다는 이점이 있다. 갈조류의 주요 구성 성분인 알긴산은 이성질체 관계에 있는 만루론산과 글루론산이 $\beta-1,4-$글리코시딕 결합으로 이루어진 고분자이며, 셀룰로오즈와 유사한 구조를 가지고 있다.

소르비톨 및 만니톨은 기존의 식품 첨가제로서의 사용 외에도 비타민 C, 프로플렌 글리콜, 에틸렌 글리콜 등의 글리콜, 고분자의 단량체 등의 생산에 사용될 수 있는 고부가가치 플랫폼 화합물이다. 소르비톨의 상업적 생산은 니켈 기반 촉매 상에서 녹말 및 셀룰로오즈 등의 목질계 바이오매스에서 유래되는 글루코오즈의 수소화 반응을 통해 이루어지고 있다.

본 연구에서는 해조류 유래 알긴산의 촉매적 수소화 반응을 통해 소르비톨 및 만니톨 등의 당알코올을 생성하였다. 당알코올의 선택적 생성을 위해 루테늄 기반 탄소 촉매가 불균일계 수소화 촉매로 사용되었다.

우선, 다양한 탄소 담체에 담지된 귀금속 촉매(루테늄, 팔라듐, 플래티늄, 로듐, 이리듐)가 알긴산 수소화 반응에 적용되었는데, 루테늄 기반 탄소 촉매가 가장 우수한 반응 활성을 보였다. 최고 6탄당알코올 수율은

50바의 수소를 가압하여 150도에서 12시간 동안 반응하였을 때 61%(소르비톨: 29% , 만니톨: 28%, 갈락티톨: 4%)로 얻을 수 있었다. 반면에, 팔라듐, 로듐, 플래티늄, 이리듐 기반 탄소 촉매를 사용한 경우는 다이디옥시 알돈산 또는 그 락톤의 형성이 관찰되었다. 핵자기공명분광법(^{13}C NMR)과 가스크로마토그래피-질량분석법을 통해 생성된 당알코올간의 이성화반응이 발생됨을 밝혔다. 또한 액체크로마토그래피-질량분석법을 통해 알긴산으로부터 당알코올이 생성되는 반응 경로를 제안하였다. 자세히는, 알긴산의 β-1,4-글리코시딕 결합은 무작위로 분해되며, 그로 인해 생성된 올리고머 중간체 화합물들의 환원말단 작용기(카르복실기 및 알데히드기)의 부분적 환원에 의해 부분 수소화된 중간체 화합물들이 형성된다. 최종적으로 다이머 중간체 내의 글리코시딕 결합이 분해되어 6탄당알코올이 생성이 된다. 상용 루테늄 기반 탄소 촉매는 반복된 재사용 실험에서 루테늄의 용출 및 소결에 의한 성능 저하가 나타났다.

다음으로, 탄소-탄소 결합 분해 및 당알코올의 이성화 반응을 억제하여 부반응을 줄이고자 다양한 전이금속이 첨가된 이종금속 촉매를 합성하여 알긴산 수소화 반응에 적용하였다. 다양한 루테늄 기반 이종금속 촉매 중 구리가 첨가된 루테늄-구리 촉매가 부반응을 가장 억제하는 것으로 관찰되었다. 구리 첨가의 시너지 효과를 살펴보기 위해, 구리 첨가량을 변화시켜 그 효과를 관찰하였다. 루테늄 카본 촉매에 구리를 첨가할 경우, 일산화탄소 화학흡착 분석을 통해 루테늄의 활성 표면이 구리에 의해 가려지는 것이 관찰되었다. 또한 X선 광분자 분광 분석을 통해

루테늄과 구리 사이의 전자 이동 효과가 나타나는 것이 관찰되었다. X선 흡수 분광 분석을 통해 관찰된 루테늄-구리 이종금속 클러스터는 두 금속간의 향상된 상호작용을 유발하며, 수소 spillover를 향상시키는 것이 관찰되었다. 위와 같은 특성은 구리 첨가에 의해 야기된 노출된 루테늄 활성 표면의 감소에도 불구하고, 루테늄-구리 이종금속 촉매가 높은 수소화 반응 활성을 유지할 수 있는 원인인 것으로 판단된다. Ru(5)Cu(1)/AC-N-13 촉매 상에서 50바 수소를 가압하여 180도에서 2시간 동안 알긴산 수소화 반응을 진행하였을 때, 47.4%(소르비톨: 26.9%, 만니톨: 20.5%)의 최고 6탄당알코올 수율을 얻을 수 있었다. 촉매는 구리의 용출로 인해 시너지 효과를 잃고 반복된 재사용 실험에서 활성 저하를 나타내었다.

마지막으로, 루테늄 기반 탄소 촉매의 수열 안정성 및 재사용성을 향상 시키기 위하여 질소 첨가 중형 기공 탄소 담체를 합성하여 알긴산 수소화 반응에 활용하였다. 탄소 담체 내의 질소 함량은 요소/글루코오즈의 비율 및 탄화 온도의 변화를 통해 조절할 수 있었다. 탄소 담체 내 질소의 첨가는 루테늄과 담체, 특히 pyridinic-질소 간의 상호작용을 유발하였으며, 이는 루테늄 산화물(RuO_x)의 형성에 영향을 끼쳤다. 또한 루테늄과 담체와의 상호작용은 수소 spillover 효과를 향상시키는 결과를 나타내었다. 루테늄 산화물은 당알코올 이성화 반응 및 탄소-탄소 결합 분해 등의 부반응을 억제하는 역할을 하는 것으로 관찰되었다. Ru(5)/NMC(0.1)(600) 촉매 상에서 50바 수소를 가압하여 180도에서 1시간 동안 알긴산 수소화 반응을 진행하였을 때, 50.3%(소르비톨: 24.3,

만니톨: 26.0%)의 최고 6탄당알코올 수율을 얻을 수 있었다. 질소 첨가 중형 기공 탄소 담체에 담지된 루테늄 촉매는 우수한 수열안정성을 나타내었다. 루테늄과 담체와의 강한 상호작용이 루테늄 용출과 소결을 억제한 것으로 판단된다.

본 연구에서는 루테늄 기반 탄소 촉매를 사용하여 기존의 목질계 바이오매스 자원에서 한정적으로 생산되었던 소르비톨 및 만니톨 등의 당알코올을 해조류 유래 알긴산으로부터 최초로 생성하였다. 또한 다양한 분석 기법을 활용하여 알긴산으로부터 당알코올 생성의 반응 경로를 제안하였다는 것에도 큰 의의가 있다. 본 연구를 통해 기존의 목질계 바이오매스에 국한되었던 연구 관심을 해조류 바이오매스로 환기 시킬 수 있을 것이라 기대된다.

주요어: 알긴산, 수소화 반응, 당알코올, 루테늄 촉매, 이종금속 촉매, 질소 첨가 중형 기공 탄소

학 번: 2015-30213

Bibliography

[1] K. Page, *New Renewable Energy Resources: A Guide to the Future*, World Energy Council, **1994**.

[2] G. W. Huber, S. Iborra, A. Corma, *Chemical Reviews* **2006**, *106*, 4044-4098.

[3] M. Yabushita, H. Kobayashi, A. Fukuoka, *Applied Catalysis B: Environmental* **2014**, *145*, 1-9.

[4] M. G. Mazzotta, D. Gupta, B. Saha, A. K. Patra, A. Bhaumik, M. M. Abu-Omar, *ChemSusChem* **2014**, *7*, 2342-2350.

[5] Y. Wang, W. Deng, B. Wang, Q. Zhang, X. Wan, Z. Tang, Y. Wang, C. Zhu, Z. Cao, G. Wang, H. Wan, *Nat Commun* **2013**, *4*.

[6] D. M. Alonso, J. M. R. Gallo, M. A. Mellmer, S. G. Wettstein, J. A. Dumesic, *Catalysis Science & Technology* **2013**, *3*, 927.

[7] T. A. Werpy, J. E. Holladay, J. F. White, U.S. Department of Energy ed. (Ed.: U. S. D. o. Energy), **2004**.

[8] H. Xiong, H. N. Pham, A. K. Datye, *Green Chemistry* **2014**, *16*, 4627-4643.

[9] E. Lam, J. H. T. Luong, *ACS Catalysis* **2014**, *4*, 3393-3410.

[10] T. Masakazu, T. Atsushi, O. Mai, *Nature* **2005**, *438*, 178.

[11] S. De, A. M. Balu, J. C. van der Waal, R. Luque, *ChemCatChem* **2015**, *7*, 1608-1629.

[12] G. S. Foo, A. H. Van Pelt, D. Krötschel, B. F. Sauk, A. K. Rogers, C. R. Jolly, M. M. Yung, C. Sievers, *ACS Sustainable Chemistry & Engineering* **2015**.

[13] H. Kobayashi, T. Komanoya , K. Hara, A. Fukuoka, *ChemSusChem* **2010**, *3*, 440-443.

[14] A. Corma, S. Iborra, A. Velty, *Chemical Reviews* **2007**, *107*, 2411-2502.

[15] M. Makkee, A. P. G. Kieboom, H. van Bekkum, *Starch - Stärke* **1985**, *37*, 136-141.

[16] C. Chatterjee, F. Pong, A. Sen, *Green Chemistry* **2015**, *17*, 40-71.

[17] A. Romero, E. Alonso, Á. Sastre, A. Nieto-Márquez, *Microporous and Mesoporous Materials* **2016**, *224*, 1-8.

[18] W. Zhu, H. Yang, J. Chen, C. Chen, L. Guo, H. Gan, X. Zhao, Z. Hou, *Green Chemistry* **2014**, *16*, 1534-1542.

[19] A. Negoi, K. Triantafyllidis, V. I. Parvulescu, S. M. Coman, *Catalysis Today* **2014**, *223*, 122-128.

[20] R. A. Lee, J.-M. Lavoie, *Animal Frontiers* **2013**, *3*, 6-11.

[21] S. Behera, R. Singh, R. Arora, N. K. Sharma, M. Shukla, S. Kumar, *Frontiers in Bioengineering and Biotechnology* **2015**, *2*.

[22] F. Alam, S. Mobin, H. Chowdhury, *Procedia Engineering* **2015**, *105*, 763-768.

[23] A. Martinsen, G. Skjåk-Bræk, O. Smidsrød, *Biotechnology and Bioengineering* **1989**, *33*, 79-89.

[24] J. A. Rowley, G. Madlambayan, D. J. Mooney, *Biomaterials* **1999**, *20*, 45-53.

[25] W. L. Nelson, L. H. Cretcher, *Journal of the American Chemical Society* **1929**, *51*, 1914-1922.

[26] A. D. Augst, H. J. Kong, D. J. Mooney, *Macromolecular Bioscience* **2006**, *6*, 623-633.

[27] W. Jeon, C. Ban, G. Park, H. C. Woo, D. H. Kim, *Catalysis Science &*

Technology **2016**, *6*, 1146-1156.

[28] W. Jeon, C. Ban, G. Park, J. E. Kim, H. C. Woo, D. H. Kim, *Catalysis Surveys from Asia* **2016**, *20*, 195-209.

[29] W. Jeon, C. Ban, G. Park, H. C. Woo, D. H. Kim, *Catalysis Today* **2016**, *265*, 154-162.

[30] C. Ban, W. Jeon, G. Park, H. C. Woo, D. H. Kim, *ChemCatChem* **2017**, *9*, 329-337.

[31] G. Park, W. Jeon, C. Ban, H. C. Woo, D. H. Kim, *Energy Conversion and Management* **2016**, *118*, 135-141.

[32] W. Jeon, C. Ban, J. E. Kim, H. C. Woo, D. H. Kim, *Journal of Molecular Catalysis A: Chemical* **2016**, *423*, 264-269.

[33] W. Jeon, C. Ban, G. Park, T.-K. Yu, J.-Y. Suh, H. C. Woo, D. H. Kim, *Journal of Molecular Catalysis A: Chemical* **2015**, *399*, 106-113.

[34] L. Brennan, P. Owende, *Renewable and Sustainable Energy Reviews* **2010**, *14*, 557-577.

[35] L. Yang, J. Su, S. Carl, J. G. Lynam, X. Yang, H. Lin, *Applied Catalysis B: Environmental* **2015**, *162*, 149-157.

[36] F. Llanes, F. Sauriol, F. G. Morin, A. S. Perlin, *Canadian Journal of Chemistry* **1997**, *75*, 585-590.

[37] T. Salomonsen, H. M. Jensen, F. H. Larsen, S. Steuernagel, S. B. Engelsen, *Carbohydrate Research* **2009**, *344*, 2014-2022.

[38] D. M. Alonso, S. G. Wettstein, J. A. Dumesic, *Chemical Society Reviews* **2012**, *41*, 8075-8098.

[39] E. S. Vasiliadou, A. A. Lemonidou, *Applied Catalysis A: General* **2011**, *396*,

177-185.

[40] E. P. Maris, R. J. Davis, *Journal of Catalysis* **2007**, *249*, 328-337.

[41] J.-W. Shim, S.-J. Park, S.-K. Ryu, *Carbon* **2001**, *39*, 1635-1642.

[42] C. Moreno-Castilla, M. A. Ferro-Garcia, J. P. Joly, I. Bautista-Toledo, F. Carrasco-Marin, J. Rivera-Utrilla, *Langmuir* **1995**, *11*, 4386-4392.

[43] A. T. To, P.-W. Chung, A. Katz, *Angewandte Chemie International Edition* **2015**, *54*, 11050-11053.

[44] A. Fukuoka, P. L. Dhepe, *Angewandte Chemie International Edition* **2006**, *45*, 5161-5163.

[45] W. Deng, M. Liu, X. Tan, Q. Zhang, Y. Wang, *Journal of Catalysis* **2010**, *271*, 22-32.

[46] A. Aho, S. Roggan, O. A. Simakova, T. Salmi, D. Y. Murzin, *Catalysis Today* **2015**, *241, Part B*, 195-199.

[47] S. K. Papageorgiou, E. P. Kouvelos, E. P. Favvas, A. A. Sapalidis, G. E. Romanos, F. K. Katsaros, *Carbohydrate Research* **2010**, *345*, 469-473.

[48] H. Mimura, H. Ohta, K. Akiba, Y. Onodera, *Journal of Nuclear Science and Technology* **2002**, *39*, 655-660.

[49] A. E. Irwin, C. M. De Ramos, B. E. Stout, in *Humic and Fulvic Acids, Vol. 651*, American Chemical Society, **1996**, pp. 244-258.

[50] H. Kobayashi, Y. Ito, T. Komanoya, Y. Hosaka, P. L. Dhepe, K. Kasai, K. Hara, A. Fukuoka, *Green Chemistry* **2011**, *13*, 326.

[51] N. Akiya, P. E. Savage, *Chemical Reviews* **2002**, *102*, 2725-2750.

[52] J. Hilgert, N. Meine, R. Rinaldi, F. Schüth, *Energy & Environmental Science* **2013**, *6*, 92.

[53] L. Wright, L. Hartmann, *The Journal of Organic Chemistry* **1961**, *26*, 1588-1596.

[54] P. J. C. Hausoul, L. Negahdar, K. Schute, R. Palkovits, *ChemSusChem* **2015**, *8*, 3323-3330.

[55] J. H. Sinfelt, *Journal of Catalysis* **1973**, *29*, 308-315.

[56] A. J. Rouco, G. L. Haller, J. A. Oliver, C. Kemball, *Journal of Catalysis* **1983**, *84*, 297-307.

[57] S. Bhatia, X. Wu, D. K. Sanders, B. C. Gerstein, M. Pruski, T. S. King, *Catalysis Today* **1992**, *12*, 165-175.

[58] J. Liu, L. L. Zhang, J. Zhang, T. Liu, X. S. Zhao, *Nanoscale* **2013**, *5*, 11044-11050.

[59] L. Yang, J. Su, S. Carl, J. G. Lynam, X. Yang, H. Lin, *Applied Catalysis B: Environmental* **2015**, *162*, 149-157.

[60] F. Rodríguez-reinoso, *Carbon* **1998**, *36*, 159-175.

[61] L. Chen, Y. Zhu, H. Zheng, C. Zhang, B. Zhang, Y. Li, *Journal of Molecular Catalysis A: Chemical* **2011**, *351*, 217-227.

[62] X. Zhang, L. J. Durndell, M. A. Isaacs, C. M. A. Parlett, A. F. Lee, K. Wilson, *ACS Catalysis* **2016**, *6*, 7409-7417.

[63] C. Ban, W. Jeon, H. C. Woo, D. H. Kim, *ChemSusChem* **2017**, *10*, 4891-4898.

[64] J. L. Figueiredo, *Journal of Materials Chemistry A* **2013**, *1*, 9351-9364.

[65] M. Thommes, K. Kaneko, A. V. Neimark, J. P. Olivier, F. Rodriguez-Reinoso, J. Rouquerol, K. S. Sing, *Pure and Applied Chemistry* **2015**, *87*, 1051-1069.

[66] S. Chen, H. Zhang, L. Wu, Y. Zhao, C. Huang, M. Ge, Z. Liu, *Journal of*

Materials Chemistry **2012**, *22*, 9117-9122.

[67] M. C. Schoenmaker-Stolk, J. W. Verwijs, J. J. F. Scholten, *Applied Catalysis* **1987**, *30*, 339-352.

[68] T. Jiang, Y. Zhou, S. Liang, H. Liu, B. Han, *Green Chemistry* **2009**, *11*, 1000-1006.

[69] R. Liu, B. Tesche, H. Knözinger, *Journal of Catalysis* **1991**, *129*, 402-413.

[70] J. P. Espinós, J. Morales, A. Barranco, A. Caballero, J. P. Holgado, A. R. González-Elipe, *The Journal of Physical Chemistry B* **2002**, *106*, 6921-6929.

[71] D. W. Goodman, C. H. F. Peden, *Journal of Catalysis* **1985**, *95*, 321-324.

[72] X. Wu, B. C. Gerstein, T. S. King, *Journal of Catalysis* **1990**, *121*, 271-293.

[73] Z. Wu, Y. Mao, X. Wang, M. Zhang, *Green Chemistry* **2011**, *13*, 1311-1316.

[74] E. Asedegbega-Nieto, B. Bachiller-Baeza, A. Guerrero-Ruíz, I. Rodríguez-Ramos, *Applied Catalysis A: General* **2006**, *300*, 120-129.

[75] J. Jae, W. Zheng, R. F. Lobo, D. G. Vlachos, *ChemSusChem* **2013**, *6*, 1158-1162.

[76] H. Kobayashi, H. Matsuhashi, T. Komanoya, K. Hara, A. Fukuoka, *Chemical Communications* **2011**, *47*, 2366-2368.

[77] G. Zhang, Z. Li, H. Zheng, T. Fu, Y. Ju, Y. Wang, *Applied Catalysis B: Environmental* **2015**, *179*, 95-105.

[78] J. Álvarez-Rodríguez, A. Guerrero-Ruiz, I. Rodríguez-Ramos, A. Arcoya-Martín, *Microporous and Mesoporous Materials* **2006**, *97*, 122-131.

[79] S. Galvagno, C. Crisafulli, R. Maggiore, A. Giannetto, J. Schwank, *Journal of Thermal Analysis* **1987**, *32*, 471-483.

[80] E. S. Vasiliadou, A. A. Lemonidou, *Applied Catalysis A: General* **2011**, *396*,

177-185.

[81] D. Chakraborty, C. D. Damsgaard, H. Silva, C. Conradsen, J. L. Olsen, H. W. P. Carvalho, B. Mutz, T. Bligaard, M. J. Hoffmann, J.-D. Grunwaldt, F. Studt, I. Chorkendorff, *Angewandte Chemie International Edition* **2017**, *56*, 8711-8715.

[82] C. Crisafulli, S. Galvagno, R. Maggiore, S. Scirè, A. Saeli, *Catalysis Letters* **1990**, *6*, 77-83.

[83] H. N. Pham, A. E. Anderson, R. L. Johnson, T. J. Schwartz, B. J. O'Neill, P. Duan, K. Schmidt-Rohr, J. A. Dumesic, A. K. Datye, *ACS Catalysis* **2015**, *5*, 4546-4555.

[84] I. Sádaba, M. López Granados, A. Riisager, E. Taarning, *Green Chemistry* **2015**, *17*, 4133-4145.

[85] L. He, F. Weniger, H. Neumann, M. Beller, *Angewandte Chemie International Edition* **2016**, *55*, 12582-12594.

[86] B. Choi, H. Yoon, I.-S. Park, J. Jang, Y.-E. Sung, *Carbon* **2007**, *45*, 2496-2501.

[87] W. Xia, *Catalysis Science & Technology* **2016**, *6*, 630-644.

[88] M. N. Groves, A. S. W. Chan, C. Malardier-Jugroot, M. Jugroot, *Chemical Physics Letters* **2009**, *481*, 214-219.

[89] C. Zhang, J. Sha, H. Fei, M. Liu, S. Yazdi, J. Zhang, Q. Zhong, X. Zou, N. Zhao, H. Yu, Z. Jiang, E. Ringe, B. I. Yakobson, J. Dong, D. Chen, J. M. Tour, *ACS Nano* **2017**, *11*, 6930-6941.

[90] H.-W. Liang, X. Zhuang, S. Brüller, X. Feng, K. Müllen, *Nature Communications* **2014**, *5*, 4973.

[91] D. Guo, R. Shibuya, C. Akiba, S. Saji, T. Kondo, J. Nakamura, *Science* **2016**, *351*, 361.

[92] M. Zacharska, O. Y. Podyacheva, L. S. Kibis, A. I. Boronin, B. V. Senkovskiy, E. Y. Gerasimov, O. P. Taran, A. B. Ayusheev, V. N. Parmon, J. J. Leahy, D. A. Bulushev, *ChemCatChem* **2015**, *7*, 2910-2917.

[93] L. Wang, B. Zhang, X. Meng, D. S. Su, F.-S. Xiao, *ChemSusChem* **2014**, *7*, 1537-1541.

[94] M. Tang, J. Deng, M. Li, X. Li, H. Li, Z. Chen, Y. Wang, *Green Chemistry* **2016**, *18*, 6082-6090.

[95] A. B. Ayusheev, O. P. Taran, I. A. Seryak, O. Y. Podyacheva, C. Descorme, M. Besson, L. S. Kibis, A. I. Boronin, A. I. Romanenko, Z. R. Ismagilov, V. Parmon, *Applied Catalysis B: Environmental* **2014**, *146*, 177-185.

[96] Q.-Y. Bi, J.-D. Lin, Y.-M. Liu, H.-Y. He, F.-Q. Huang, Y. Cao, *Angewandte Chemie International Edition* **2016**, *55*, 11849-11853.

[97] L. Roldán, Y. Marco, E. García-Bordejé, *ChemSusChem* **2017**, *10*, 1139-1144.

[98] D. A. Bulushev, M. Zacharska, A. S. Lisitsyn, O. Y. Podyacheva, F. S. Hage, Q. M. Ramasse, U. Bangert, L. G. Bulusheva, *ACS Catalysis* **2016**, *6*, 3442-3451.

[99] W. Liu, Y. Chen, H. Qi, L. Zhang, W. Yan, X. Liu, X. Yang, S. Miao, W. Wang, C. Liu, A. Wang, J. Li, T. Zhang, *Angewandte Chemie International Edition* **2018**, *57*, 7071-7075.

[100] J. Hu, Z. Zhang, F. Wang, S. Zheng, J. Cai, J. Qin, W. Liu, S. Liang, X. Jiang, *RSC Advances* **2016**, *6*, 101544-101551.

[101] J. Zhu, L. Gan, B. Li, X. Yang, *Korean Journal of Chemical Engineering* **2017**, *34*, 110-117.

[102] W. He, C. Jiang, J. Wang, L. Lu, *Angewandte Chemie International Edition* **2014**, *53*, 9503-9507.

[103] W. Shen, W. Fan, *Journal of Materials Chemistry A* **2013**, *1*, 999-1013.

[104] Y.-H. Li, T.-H. Hung, C.-W. Chen, *Carbon* **2009**, *47*, 850-855.

[105] Y. Zhou, R. Pasquarelli, T. Holme, J. Berry, D. Ginley, R. O'Hayre, *Journal of Materials Chemistry* **2009**, *19*, 7830-7838.

[106] Y. Hu, G. Jiang, G. Xu, X. Mu, *Molecular Catalysis* **2018**, *445*, 316-326.

[107] P. G. J. Koopman, A. P. G. Kieboom, H. van Bekkum, J. W. E. Coenen, *Carbon* **1979**, *17*, 399-402.

[108] K. Liu, X. Huang, E. A. Pidko, E. J. M. Hensen, *ChemCatChem* **2018**, *10*, 810-817.

[109] M. Verziu, A. Tirsoaga, B. Cojocaru, C. Bucur, B. Tudora, A. Richel, M. Aguedo, A. Samikannu, J. P. Mikkola, *Molecular Catalysis* **2018**, *450*, 65-76.

[110] R. Lanza, S. G. Järås, P. Canu, *Applied Catalysis A: General* **2007**, *325*, 57-67.

[111] K. L. Deutsch, D. G. Lahr, B. H. Shanks, *Green Chemistry* **2012**, *14*, 1635-1642.

[112] N. Li, G. W. Huber, *Journal of Catalysis* **2010**, *270*, 48-59.

[113] K. Wang, M. C. Hawley, T. D. Furney, *Industrial & Engineering Chemistry Research* **1995**, *34*, 3766-3770.

[114] A. E. Irwin, C. M. De Ramos, B. E. Stout, in *Humic and Fulvic Acids, Vol.*

651, American Chemical Society, **1996**, pp. 244-258.

[115] E. P. Maris, W. C. Ketchie, V. Oleshko, R. J. Davis, *The Journal of Physical Chemistry B* **2006**, *110*, 7869-7876.

[116] R. Arrigo, M. E. Schuster, Z. Xie, Y. Yi, G. Wowsnick, L. L. Sun, K. E. Hermann, M. Friedrich, P. Kast, M. Hävecker, A. Knop-Gericke, R. Schlögl, *ACS Catalysis* **2015**, *5*, 2740-2753.

[117] F. Su, L. Lv, F. Y. Lee, T. Liu, A. I. Cooper, X. S. Zhao, *Journal of the American Chemical Society* **2007**, *129*, 14213-14223.

[118] T. Ishihara, K. Harada, K. Eguchi, H. Arai, *Journal of Catalysis* **1992**, *136*, 161-169.

[119] B. Lin, Y. Guo, R. Liu, X. Wang, J. Ni, J. Lin, L. Jiang, *Industrial & Engineering Chemistry Research* **2018**, *57*, 2819-2828.

[120] B. Lin, R. Wang, J. Lin, J. Ni, K. Wei, *Catalysis Letters* **2011**, *141*, 1557.